

# A Near-Infrared Stellar Census of Blue Compact Dwarf Galaxies: NICMOS<sup>1</sup> Detection of Red Giant Stars in the Wolf-Rayet Galaxy Mrk 178

Regina E. Schulte-Ladbeck

*University of Pittsburgh, Pittsburgh, PA 15260, USA*

rsl@phyast.pitt.edu

Ulrich Hopp

*Universitätssternwarte München, München, FRG*

hopp@usm.uni-muenchen.de

Laura Greggio

*Osservatorio Astronomico di Bologna, Bologna, Italy, and Universitätssternwarte München,  
München, FRG*

greggio@usm.uni-muenchen.de

Mary M. Crone

*Skidmore College, Saratoga Springs, NY 12866, USA*

mcrone@skidmore.edu

## ABSTRACT

We observed the Blue Compact Dwarf/Wolf-Rayet galaxy Mrk 178 with the NICMOS camera aboard HST. The galaxy is well resolved into individual stars in the near-IR; photometry in J and H yields color-magnitude diagrams containing 791 individual point sources. We discuss the stellar content, drawing particular attention to the intermediate age and/or old stars.

Mrk 178 is only the second Blue Compact Dwarf galaxy in which the red giant branch has been resolved, indicating stars with ages of at least 1-2 Gyr. This allows us to derive a distance of  $\geq 4.2(\pm 0.5)$  Mpc. The near-IR color-magnitude diagram also exhibits an abundance of luminous, asymptotic giant branch stars. We find that this requires vigorous star formation several hundred Myr ago. Some candidate carbon stars are identified via their extreme near-IR color.

---

<sup>1</sup>Based on observations made with the NASA/ESA Hubble Space Telescope obtained from the Space Telescope Science Institute, which is operated by the Association of Universities for Research in Astronomy, Inc., under NASA contract NAS 5-26555.

We argue that Mrk 178 is fundamentally an old galaxy, based on the NICMOS detection of red giants underlying the blue, starburst core, and its extended, faint halo of redder color.

*Subject headings:* Galaxies: compact — galaxies: dwarf — galaxies: evolution — galaxies: individual (Mrk 178 = UGC 6541) — galaxies: stellar content — stars: AGB, carbon

## 1. Introduction

Within the well-accepted framework of hierarchical collapse, today’s dwarf galaxies are considered to be the non-merged remnants of small-scale primordial density fluctuations in the early Universe (White & Rees 1978, Dekel & Silk 1986, Ikeuchi & Norman 1987). Dwarf galaxies are still the most common kind of galaxy in the Universe today, and they may have been even more abundant in the recent past when they presumably were part of the Faint Blue Excess (e.g., Ellis 1997, Marzke & Da Costa 1997). What then, is the relationship between today’s dwarf population and the dwarf-like component of the faint-blue galaxies undergoing strong starbursts at  $z \approx 0.5$ -1 (Koo et al. 1994, 1995, Ferguson & Babul 1998, Guzmán et al. 1998)? At the present epoch, we observe two morphologically distinct kinds of dwarf galaxies: the early-type dwarfs (dSph and dE) which, broadly speaking, contain mainly old stars, little or no gas, and are generally situated in galaxy clusters; and the late-type dwarfs (dIrr and BCD) which are gas rich and actively forming stars. These are generally found in low-density environments with some even in galaxy voids (Popescu, Hopp & Rosa 1999). How have dark-matter content, astration rate, gas cycling and environment produced this range of properties in the dwarf galaxy population we see today (e.g. Dekel & Silk 1986, Skillman & Bender 1995, Ferrara & Tolstoy 2000)?

It has been a long-standing question whether Blue Compact Dwarf (BCD) galaxies are old galaxies which made their first generation of stars at high redshift and are currently experiencing a burst of star formation, or young galaxies which are forming their very first stars at the present epoch (Searle & Sargent 1972, Searle, Sargent & Bagnuolo 1973, Kunth, Maurogordato & Vigroux 1988, Thuan 1991, Izotov & Thuan 1999). This question is prompted by the combination of low metal abundances (for ionized gas) and the high present-day star-formation rates in BCDs. Abundance determinations have traditionally been used to gain insight into the histories of BCDs. Izotov & Thuan (1999) recently compared the chemical abundances of the ionized gas of 50 BCDs with theoretical stellar nucleosynthetic yields, and concluded that most BCDs are young. Specifically, they argue that galaxies with metallicities (oxygen abundances)  $Z \leq Z_{\odot}/20$  are experiencing their first starburst and are no older than  $\approx 40$  Myr to 100 Myr, so-called “primeval” galaxies. For those BCDs with  $Z \leq Z_{\odot}/5$ , they suggest an upper age limit of 1-2 Gyr.

A new avenue to age-date BCDs has opened up with the advent of HST, which allows nearby BCDs to be resolved into individual stars. Color-magnitude diagrams (CMD) have been interpreted

to indicate that some low metallicity BCDs are neither primeval nor young. For example, the present starburst is not the first one to occur in the famous I Zw 18 (Aloisi, Tosi & Greggio 1999), the most metal-poor BCD known ( $\approx Z_{\odot}/50$ ), and there is evidence that VII Zw 403 ( $\approx Z_{\odot}/20$ ) may even contain an ancient stellar population (e.g. Schulte-Ladbeck, Crone & Hopp 1998, hereafter SCH98).

The disagreement in the star-formation histories (SFH) derived from spectroscopy of the ionized gas and photometry of the stellar content is a significant concern. CMDs can only be obtained for very nearby galaxies, while emission-line spectroscopy can be used to investigate star-forming galaxies at high redshift. It is therefore important to understand the data on local galaxies.

CMD studies use stars as clocks to provide a measure of a galaxy’s age. A very young galaxy may be recognized by its high-mass stars, which live only for a few tens of Myr. When stars that are older than a few hundred Myr are detected — typically intermediate-mass stars on the early asymptotic giant branch (E-AGB) or in the thermally pulsing AGB phase (TP-AGB) — the galaxy is at least about 0.5 Gyr old. Note that in star clusters and early-type galaxies, AGB stars of a much lower luminosity and mass are observed, possibly indicating intermediate ages of up to 10 Gyr. We discuss AGB stars further below. In star-forming galaxies, many luminous AGB stars of comparatively high mass are observed, and they swamp the contribution of the low-mass upper AGB stars near the tip of the red giant branch (TRGB). The red-giant-branch (RGB) appears after an evolutionary time scale of about 1 Gyr (Sweigart, Greggio & Renzini 1990, Bressan, Chiosi & Fagotto 1994). This result is robust and does not depend much on the initial metallicity of the population. Hence, when a galaxy exhibits a well-populated red giant branch, it is at least 1-2 Gyr old. The unambiguous detection of stars much older than 1-2 Gyr is a problem, because BCDs are situated at large enough distances to prevent direct access to old main-sequence turnoffs, or horizontal-branch stars, with today’s telescopes. We refer to this limitation as the “1-2 Gyr frontier”. In any event, an old galaxy would be one that contains stars with ages in excess of 10 Gyr. The detection of a well defined TRGB is regarded as a necessary, but not a sufficient condition to establish the presence of old stars (Da Costa 1994).

In this paper we report on our NIC2 observations of the BCD Mrk 178 = UGC 6541. The advantage of using NICMOS to search for intermediate-mass/old stars in this Wolf-Rayet (W-R) galaxy is that the spectral energy distribution of such stars peaks in the near-IR. In Figure 1, we display the Digitized Sky Survey (DSS) 103a-E image of Mrk 178. This image suggests that Mrk 178 belongs to the type “iE” BCDs in the classification of Loose & Thuan (1986). In iE BCDs, the bright blue star-forming regions are situated near the center of an elliptical, faint red background sheet. The contour maps of multi-filter CCD images by González-Riestra, Rego & Zamorano (1988) support this classification as well. Mrk 178 was recently resolved into its brightest stars from the ground, resulting in a distance modulus of 27.73, or a distance of 3.5 Mpc (Georgiev, Karachentsev & Tikhonov 1997). The present-day metallicity derived from emission-line spectroscopy of the ionized gas is  $12+\log(\text{O}/\text{H}) = 7.950_{-0.021}^{+0.020}$  (Kobulnicky & Skillman 1996), or  $\approx Z_{\odot}/10$ . Mrk 178 is located at the peak of the metallicity distribution observed for BCDs (compared with the sample

of Izotov & Thuan 1999). There is evidence for active star-formation over the last 10 Myr from the presence of emission lines in the spectra. Observation of the W-R bump in the spectrum of the younger of two centrally located H-II regions (González-Riestra, Rego & Zamorano 1988) suggests that this activity is on-going. The galaxy has an H-I detection in the survey of Thuan & Martin (1981) which, at the distance of 4.2 Mpc which we derive in this paper, translates into an H-I mass of about  $1.4 \times 10^7 M_{\odot}$ . By all accounts then, Mrk 178 appears to be a typical representative of the BCD class.

## 2. Observations and reductions

We observed Mrk 178 on 1998 September 27 as part of GO program 7859. The NIC2 camera, which has a field of view of  $19''.2 \times 19''.2$ , was centered at (J2000) R.A. 11:33:28.82 and Dec. 49:14:12.4 on the SE knot, the brighter of two prominent star-forming regions (cf. González-Riestra, Rego & Zamorano 1988). The galaxy UGC 6538 is nearby on the sky, but while Mrk 178 has a heliocentric velocity of  $249(\pm 4) \text{ km s}^{-1}$ , UGC 6538 has a much larger recession velocity of  $3180 \text{ km s}^{-1}$  (see NED), and is physically unrelated. The classification of Mrk 178 as a “galaxy pair”, which is sometimes found in the literature, is not justified. Instead, Mrk 178 appears to be an isolated star-forming dwarf.

The data were obtained in the F110W and the F160W filters, which are similar to the ground-based J and H bands. Information about the observations can be gleaned directly from the STScI WWW pages linked to program ID 7859; this provides a detailed observing log. The total integration time was about 5568 s in F110W, and 2880 s in F160W. Specifically, the data set in F110W consists of six individual exposures. In the first set of three, the exposure times were 895.956 s per exposure, in set two (less acquisition overhead in second orbit), they were 959.953 s per exposure. The F160W observations consist of one set of three exposure, each 959.953 s in duration. Between individual exposures of a set, the camera was dithered by  $1''$  in the X direction using the canned, XSTRIP-DITH pattern. All exposures were read out in MULTIACCUM mode; cosmic rays were rejected.

The color image is displayed as Figure 2, and shows how well Mrk 178 resolves into single stars with NIC2. The data were reduced following the steps outlined in SHGC99. Our major concern was to reproduce as closely as possible the reduction of the VII Zw 403 data, from which we derived our distance calibration. The calibration files and the pedestal-removal software used reflect the status of knowledge as of mid 1999. We used a set of temperature-dependent dark current files for the reduction of all data. These dark reference files correct for shading, which is a temperature-dependent component of detector bias. We also investigated all of the data in our program for cosmic-ray persistence, and pedestal problems. We used M. Dickinson’s software for pedestal removal. Even after the above re-reduction steps were carried out, the data had a spatially non-uniform background, a feature that poses a problem for DAOPHOT (Stetson, Davis, & Crabtree 1990). Therefore, the star-subtracted background was smoothed as described in SHGC99. We used

the combined, mosaicked images that resulted from calnibc for the photometry, since we found that there was no significant difference to the DAOPHOT PSF photometry using the drizzle procedure. We checked the resulting photometry by eye, to make sure that we did not pick up spurious sources due to blending.

The conversion of PSF photometry to absolute photometry in the HST Vegamag system was carried out following the prescriptions given in the NICMOS Photometric Calibration Cookbook. We determined the countrates of 9 (F110W) and 7 (F160W) well isolated stars (from the list of stars used to define the PSF for DAOPHOT). These countrates were measured in the aperture of  $0''.5$  to which the NICMOS photometric calibration is referred. The sky-background was measured in a ring between  $0''.65$  and  $6''.0$  from the respective star. To convert the countrates to fluxes, we used the following photometric keywords: for F110W,  $\text{PHOTFNU} = 1.823290 \times 10^{-6} \text{ Jy sec DN}^{-1}$ , for F160W,  $\text{PHOTFNU} = 2.070057 \times 10^{-6} \text{ Jy sec DN}^{-1}$ . We applied the correction factor of 1.15 in flux (or 0.1517 in mags) to the nominal infinite aperture. We adopted fluxes of 1898 Jy in F110W, and 1113 Jy in F160W, for the zeropoints of the HST Vegamag system. We then compared the photometry of the PSF stars in this system to their PSF photometry in our internal, instrumental system. The resulting transformations were applied to the DAOPHOT star lists.

There are 1557 individual point sources detected in F110W, and 1087 sources detected in F160W. Figure 3 shows the error distributions for the photometry, and Figure 4 shows the results of tests which investigate the incompleteness of our photometry. The results indicate that the limiting magnitude is about 26.5 in F110W and 25.5 in F160W, and that the data are better than 90% complete to a magnitude of about 24.0 in F110W and 23.3 in F160W.

The completeness tests used the DAOPHOT/ADDSTAR routine. Tests were done in one-magnitude bins, ranging from  $\approx 6$  mag above the detection limit to almost the detection limit. In every simulation, 100 artificial stars were added, and then the manipulated frames were measured in the same way as the original ones. For every magnitude bin in every band, 10 simulations were carried out. The final star list of each test was cross-correlated with the input list of artificial stars, and from the difference, the completeness factors and errors shown in Fig. 4 were calculated.

In the faintest magnitude bin, very few stars (5-13) were recovered. There is indeed a non-zero chance that a faint artificial star is put on top of a noise peak (or on another faint, but real object), which make it detectable, while all others are not. Looking at the distribution of input-magnitude versus output-magnitude lists of the tests, one gets a more-or-less Gaussian error distribution for the brighter objects, which widens more and more going fainter, as expected. When approaching the detection limit, this distribution has a highly non-symmetric appearance: more and more test stars come back brighter than their input flux. In the faintest bin, all recovered stars have brighter magnitudes than their input, pointing clearly to the above effect. Naturally, this also happens in the real data. Further, at the very detection limit, unusually powerful noise peaks of the right shape may enter the target list. Therefore, all sources in the faintest magnitude bin above the detection limit are highly questionable. This must be considered in the discussion of the data. As the total

number of objects in the bins affected by blending is small, they should have little influence on the interpretation of the data, or the CMD simulations.

We merged the two star lists requiring a positional source coincidence of better than 1.5 pixels or  $\approx 0''.1$  (determined from cross-correlation experiments). There are 791 objects with coincident positions in F110W and F160W. Figure 5 shows CMDs constructed from these data.

### 3. Results

The foreground galactic extinction towards Mrk 178 is negligible:  $A_B=0.000$  from H-I maps (Burstein & Heiles 1984);  $A_B=0.077$ , which corresponds to  $A_J=0.016$  and  $A_H=0.010$  from IRAS maps (Schlegel et al. 1998, and see NED). Having only two bands available to us, we cannot investigate the internal extinction using a two-color diagram, but we assume the effect is small in the near-IR. Because the field of the NIC2 camera is so small and because Mrk 178 is situated at high galactic latitude ( $63^\circ 3'$ ), we expect the contamination of the CMDs by galactic foreground stars to be very small. Thus, it is relatively straightforward to interpret the CMDs.

The CMDs of Fig. 5 are characterized by a strong red plume, and a comparatively weak blue plume. Most of the stars in these CMDs appear at red colors and faint magnitudes; *this is the red tangle which contains the RGB*. Depending on the specific star-formation history (SFH), some combination of AGB stars and even blue-loop (BL) stars can also contribute to this feature. The solid line of Fig. 5 marks the magnitude at which we identify the TRGB (see below). Above the TRGB, we expect to see AGB stars and red supergiants (RSG). In Mrk 178, there is a considerable number of red stars above the RGB, which we suspect are AGB stars. Above the red tangle, the linear feature extending to bright magnitudes is presumably dominated by RSGs, whereas the reddest of the bright stars, which form a fan-shaped grouping in the CMDs, are likely to be mainly AGB stars. The blue plume can include main-sequence (MS), BL, and blue-supergiant (BSG) stars.

#### 3.1. The distance

The core helium flash of low mass stars occurs at a constant bolometric magnitude over a wide range of stellar masses and metallicities. The TRGB has therefore been successfully calibrated as a distance indicator for galaxies (Lee, Freedman & Madore 1983). In I-band luminosity functions, the TRGB is found as a sharp rise in stellar frequency towards fainter magnitudes. The bolometric correction has been determined empirically from globular cluster observations and the V-I color is well calibrated as a function of metallicity. After applying the bolometric correction, the distance modulus of a galaxy may be derived. This is the basis of the I-band TRGB method.

While RGB stars are much brighter in J and H than in I and V, affording detectability of the TRGB to larger distances, there are several disadvantages in using the TRGB in J and H as a

distance indicator. In SHGC99, we investigated the TRGB in J and H using both stellar evolution models and globular cluster observations. In stellar models, the TRGB in both J and H depends on metallicity; at low metallicity the absolute magnitudes at the TRGB are fainter than at high metallicity. This is illustrated in Fig. 8 of SHGC99. According to the Padova stellar models, the variation of the absolute H-band magnitude with metallicity is small for low metallicities, indicating that the H-band might be the better of the two bands to use for determining distances. In addition, there is a large uncertainty of the ground calibration of the J band, which prompted us to discard the TRGB in J in the ground system as a useful distance indicator.

In what follows we discuss the TRGB based both on the F110W, F160W data and the transformed, H-band data. We also consider that we have no prior knowledge of the metallicity of the RGB stars in Mrk 178, and give both our preferred “short” distance based on the assumption of a low-metallicity RGB, and a “long” distance allowing the H-band metallicity to be as high as solar.

In order to determine the distance of Mrk 178, we need to measure the brightness of the TRGB. This is usually accomplished by finding the steepest gradient in the luminosity function of the stars in the red plume, e.g., by applying an edge-detecting, Sobel filter. In the case of Mrk 178 the situation is complicated by the fact that this galaxy has a prominent population of luminous AGB stars, which overlaps the RGB population near the TRGB. The net effect is that the contrast in stellar number counts at the TRGB is less pronounced, and the TRGB itself is harder to pin down. We combined information from luminosity functions with our evaluation of the CMDs, to settle on a best estimate for the magnitude at the TRGB in Mrk 178. In Figure 6, we show the luminosity functions for red stars in the color interval  $0.75 < (F110W-F160W) < 1.5$ , in magnitude bins of 0.1. In the F110W filter, there is a sharp rise at a magnitude of 24, which we identify with the TRGB. It is not entirely clear where to identify the TRGB in F160W; a rise is seen across several bins. Luckily, the CMDs can be used to help understand the onset of the TRGB. While the feature which we consider to be the TRGB remains constant in magnitude over a wide color range in the  $[(F110W-F160W), F110W]$  CMD, it is slanted in the  $[(F110W-F160W), F160W]$  CMD. The plateau in the  $[(F110W-F160W), F110W]$  CMD of Fig. 5 translates into a sharp jump in the luminosity function in the F110W filter in Fig. 6, while the slanted TRGB in the  $[(F110W-F160W), F160W]$  CMD translates into a more gradual rise in the F160W luminosity function. This is reflected by our error estimates. Using both the luminosity functions and the CMDs for guidance, we determine the following magnitudes at the TRGB:

$$m_{F110W_o,TRGB} = 24.00 \pm 0.05 \text{ and}$$

$$m_{F160W_o,TRGB} = 22.7 \pm 0.2.$$

The errors reflect our estimates as to how well we think that we can locate the TRGB in the data. We notice that we find the TRGB at magnitudes where the data are still 90% complete or better. The distance modulus of Mrk 178 may be derived using the calibration which we established for VII Zw 403 in SHGC99

$$M_{F110W_o,TRGB} = -4.28 \pm 0.10 \pm 0.18 \text{ and}$$

$$M_{F160W_o,TRGB} = -5.43 \pm 0.10 \pm 0.18$$

where the first error is the statistical error and is dominated by how well we can determine the location of the TRGB in VII Zw 403, and the second one is the systematic error primarily due to the RR Lyrae distance calibration of the TRGB (see SCH98). In what follows, we will not give the systematic error again explicitly; the errors quoted are those that refer to our statistical errors. Applying this calibration directly provides the following distance moduli for Mrk 178 using F110W and F160W, respectively:  $28.28(\pm 0.11)$  and  $28.13(\pm 0.22)$ , corresponding to distances of  $4.5(\pm 0.2)$  Mpc and  $4.2^{+0.5}_{-0.4}$  Mpc. Application of the above calibration assumes the RGB stars of Mrk 178 have the same metallicity as those in VII Zw 403 ( $[\text{Fe}/\text{H}]=-1.92$ ).

We derive a more general calibration over a wider range of metallicities by comparing the H-band magnitude of the TRGB of VII Zw 403 with that of GCs and stellar evolution models (cf. SHGC99). The TRGB in H is a constant as a function of metallicity for a wide range of low metallicities

$$M_{H_o,TRGB} = -5.5 \pm 0.1$$

for  $-2.3 < [\text{Fe}/\text{H}] < -1.5$ .

We employ the equations given in SHGC99 to transform from F110W, F160W to ground-based J and H. Figure 7 shows the transformed CMDs, on the same scale as those of Fig. 5 for comparison. The transformation has the effect of shifting the red plume closer to the blue plume. The transformed H magnitude at the TRGB is

$$m_{H_o,TRGB} = 22.6 \pm 0.1.$$

We obtain an H-band based distance modulus of  $28.1(\pm 0.26)$ , corresponding to a distance of  $4.2(\pm 0.5)$  Mpc.

If the RGB population of Mrk 178 is more metal-rich, the TRGB indicates a larger distance modulus. If the RGB stars of Mrk 178 have solar metallicity, then  $M_{H_o,TRGB}$  is  $-6.2$  in the stellar evolution models of the Padova group (e.g. Fagotto et al. 1994, Bertelli et al. 1994). This leads to a distance modulus of 28.8, or a distance of about 5.8 Mpc. It is not entirely clear how well the metallicity dependence of the models compares with observations. In Figure 11 of SHGC99, we compare the Padova models with observations of globular clusters (GC). While there is good agreement for the lowest metallicities, the available data do not help to elucidate what  $M_{H_o,TRGB}$  is at higher metallicities; there is too much scatter.

Our minimum distance estimated from the TRGB in the near-IR using the low-metallicity assumption, 4.2 Mpc, is slightly larger than the distance derived by Georgiev, Karachentsev &



Tikhonov (1997), 3.5 Mpc. This is not surprising, mostly because the supergiant distance method suffers from large uncertainties (see Schulte-Ladbeck & Hopp 1998). Our errors are primarily due to the large component of AGB stars near the RGB tip. This problem could have been avoided in principle, by pointing the NIC2 into the background sheet of Mrk 178. However, we decided to observe on the star-forming regions to minimize the risk — if there were no RGB or if the galaxy were more distant, we might have ended up not detecting any stars in Mrk 178. We studied luminosity functions using only spatial regions near the rim of the NIC2 chip, and there was no significant difference to where we located the TRGB in that data compared to using data from the center of the chip.

In the subsequent sections of this paper, we compare the Mrk 178 data with theoretical tracks and synthetic CMDs. We point out that any “high-metallicity” assumption for the RGB corresponds to a “long” distance. From our previous work, we have a slight preference for the “low-metallicity” assumption. However, without better knowledge of the metallicity of the RGB stars in Mrk 178, the “low-metallicity” or “short” distance used here must be regarded as a lower limit to the true distance of Mrk 178.

### 3.2. Distance-dependent global parameters

We rescaled the global parameters to a distance of 4.2 Mpc ( $m-M=28.1$ ). At this distance, the H-I flux measured by Thuan & Martin (1981) corresponds to an H-I mass of  $1.4 \times 10^7 M_{\odot}$ . González-Riestra, Rego & Zamorano (1988) measured the  $H_{\alpha}$  fluxes of the two prominent H-II regions. Since these are spectroscopically derived fluxes, they probably missed some flux outside of the measurement aperture; the sum of the two fluxes will only give a lower limit on the star-formation rate (SFR) of Mrk 178. We derive  $L(H_{\alpha}) > 3.9 \times 10^{38}$  ergs  $s^{-1}$ , and, following Hunter & Gallagher (1986) who adopt the Salpeter IMF from 0.1 to  $100 M_{\odot}$ , the SFR is  $> 0.003 M_{\odot} \text{ yr}^{-1}$ . New imaging data in  $H_{\alpha}$  (Hunter 2000) suggest a value of  $> 0.008 M_{\odot} \text{ yr}^{-1}$  (assuming zero extinction). The diameter of Mrk 178 ( $D_{25}$  from the RC3) is  $1'.23$ . This corresponds to a linear size of 1.5 kpc. The total galaxy colors in the RC3 are listed as  $B-V=0.35$ ,  $U-B=-0.3$ . These are rather typical colors compared to the colors of the dIrr/BCD sample considered by Schulte-Ladbeck & Hopp (1998). The total apparent blue magnitude from the RC3, 14.50, translates into a total absolute blue magnitude of  $-13.60$ . This corresponds to a blue luminosity of about  $4 \times 10^7 L_{\odot}$  (for  $M_{B,\odot}=5.41$ ). The ratio of the H-I mass to the blue luminosity (in solar units) is 0.4. This value is typical compared with the compilation of dwarf-galaxy  $M_{HI}/L_B$  ratios given in Huchtmeier, Hopp & Kuhn (1997).

### 3.3. The stellar content

In Figure 8, we display  $[(J-H)_o, H_o]$  CMDs of Mrk 178 with three values of the DAOPHOT errors in both J and H applied as a selection criterion. In comparison with Fig. 7, this shows that

many of the faint and very red stars have large photometric errors. In addition, some might well be blends, as sometimes happens near the detection limits of crowded-field photometry. What can also be seen is that even when only stars with small photometric errors are selected, the salient features of the CMD remain. In particular, the blue stars are real detections even in the near-IR. More importantly for deriving the SFH of the galaxy, the detection of AGB and RGB stars is a secure result.

In Figure 9, we overplot onto the  $[(J-H)_o, H_o]$  CMD stellar evolutionary tracks drawn from the same database which we used in SHGC99. Briefly, these tracks are based on the Padova library of stellar tracks (e.g. Fagotto et al. 1994, Bertelli et al. 1994) and the stellar atmospheres of Bessell, Castelli & Plez (1998). We employ in our discussion two sets of tracks with metallicities of  $Z=0.0004$  and  $Z=0.004$  ( $Z_{\odot}/50$  and  $Z_{\odot}/5$ , respectively.) The present-day ionized gas abundance of Mrk 178 ( $Z_{\odot}/10$ ) is bracketed by these two, and so these tracks are a reasonable approximation for any “high-metallicity” and “low-metallicity” stellar population which we might expect to find. Note that in the low- $Z$  case we assume the short distance modulus and for the high- $Z$  case we assume a long distance modulus of 28.8. The tracks do not extend to the extremely red colors observed for some of the asymptotic giants; this is due to the truncation at the first thermal pulse of the electronically available Padova tracks (Fagotto et al. 1994).

When converting the Padova tracks to the observational plane, we employed a different set of stellar atmospheres than the one used by the Padova group. Our low-metallicity tracks ( $Z=0.0004$ ) have  $M_{H_o,TRGB}$  in good agreement with the original Padova tracks. Both sets of tracks with different atmospheres yield the same distance. For the  $Z=0.004$  tracks, our  $M_{H_o,TRGB}$  is about 0.1 magnitudes brighter than the Padova one. This is not in conflict with the observations (see Fig. 11 of SHGC99). We now trace through the evidence for both recent star formation and an older underlying population using the CMD of Fig. 9.

There are three indicators of present-day star-forming activity in Mrk 178. First, spectroscopic evidence exists for the presence of W-R stars (González-Riestra, Rego & Zamorano 1988). Star-formation in Mrk 178 must thus have been active within the last few Myr. Given the present-day metallicity of Mrk 178, stars with very high masses, roughly  $50 M_{\odot}$  and higher, are expected to be above the cut-off mass for the W-R channel (see Maeder & Conti 1994). Second, the H-II regions indicate the presence of ionizing, young and massive stars with ages of up to 10 Myr. Third, the blue plume of the CMD presumably contains massive MS stars and BSGs. The blue plume is fairly weak in Mrk 178. However, a comparison of the observations with the stellar-evolution tracks indicates that this is because the observations barely contain the top of the MS. The MS turnoff of the  $9 M_{\odot}$  track, for example, is already well below our detection limit.

Due to the sparsely populated blue plume of Mrk 178, we cannot tell about internal extinction within the H-II regions from these data. If anything, the effect appears to be small as the data scatter about the theoretically expected location of the upper MS.

The red plume is quite strong in Mrk 178. It can be split into regions above and below the

TRGB. The luminous portion of the red plume can in principle be composed of RSG stars and AGB stars. Whereas optical colors, or optical—near-IR colors (see SHGC99), separate well many AGB stars from the RSG stars, these objects tend to overlap more closely in  $(J-H)_o$ . This observation is consistent with stellar-evolution models; comparing the two sets of tracks with the data indicates an age-metallicity degeneracy. We could interpret the grouping of high-luminosity stars at  $M_{H_o}$  of about -8 and colors of  $(J-H)_o \approx 0.7$  either as intermediate-mass stars, or as high-mass stars. Thus the possible age-range spans from a few ten, to a few hundred Myr.

We can more clearly separate the AGB from the RSG stars observationally when they are redder than  $(J-H)_o$  of about 1.0, in the regime of the thermally pulsing, or TP-AGB phase. Indeed we see in Figs. 8 and 9 a few stars which have small errors, are bright, and are as red as  $(J-H)_o \approx 1.5$ . TP-AGB stars in principle probe ages of a few hundred Myr to a few Gyr.

The  $Z=0.004$  tracks provide a fairly good description of the luminous stellar content of Mrk 178. The  $Z=0.004$  low-mass tracks are, however, too red at the TRGB. The lifetime of the  $1 M_{\odot}$  star of this metallicity is 8.5 Gyr. Tracks of lower masses, and older ages, fall to the right of this track. This would have the effect of producing a red tangle which is too red to match the observations. This is illustrated by the synthetic CMDs discussed below. The low-mass tracks at low-metallicity ( $Z=0.0004$ ), on the other hand, on which we find stars as old as the Hubble time, fall near the center of the distribution of stars in the red tangle. The fainter and bluer portion of the red tangle could contain intermediate mass stars (with ages as young as 300 Myr). Toward high masses (and young ages), the tracks are bluer and the TRGBs fainter. This may be what gives the red tangle its characteristic, slanted tip shape towards blue colors in  $[(J-H)_o, H_o]$  CMDs. The red tangle may thus in principle comprise a mix of old and intermediate-mass stars of low metallicity, as well as intermediate-mass stars of higher metallicity. While the red tangle could contain stars as old as the Hubble time, we cannot clearly pinpoint any ancient stars in these data.

#### 4. Discussion

We are interested in finding out whether Mrk 178 is fundamentally young or old. To this end, we provide a variety of arguments that help us glean its SFH. There is no doubt that stars of ages between 1-2 Gyr are present, and hence Mrk 178 cannot be a primeval galaxy. Without stars in the 1-2 Gyr range of ages, we would not see an RGB or get a defined TRGB. Whether or not Mrk 178 is an ancient galaxy is another problem entirely, because the 1-2 Gyr frontier prevents us from directly identifying the old stars. However, we build a series of arguments which indicate that the presence of ancient stars in Mrk 178 is probable. These include the presence of carbon stars, the galaxy’s morphology, and constraints on the total mass in stars derived from synthetic CMDs.

#### 4.1. Comparison with other galaxies

We recently presented and discussed CMDs of VII Zw 403 (SCH98, SHGC99, Schulte-Ladbeck et al. 1999, hereafter SHCG99). HST/WFPC2 observations of this very nearby BCD allowed us to demonstrate the presence of intermediate-age AGB stars, and of a radial stellar population gradient from the young “core”, to the old “halo”. The extended, old halo exhibits no young stars and a narrow RGB which is consistent with the presence of low-metallicity, low-mass, and consequently, truly old stars. We argue that this galaxy is at least several Gyr old, and possibly older than 10 Gyr.

Optical CMDs are relatively well-understood. To take advantage of this knowledge in interpreting near-IR CMDs, in SHGC99 we cross-identified the stars found in the optical observations of VII Zw 403 with those found in the near-IR. The results are illustrated in Fig. 10, where we color-code stars based on their location in the  $[(V-I)_o, I_o]$  CMD. We color the stars in the blue plume in blue, the stars in the red plume above the TRGB in magenta, and stars in the red tangle below the TRGB in red. We show stars in the red tail in black; this region of the  $[(V-I)_o, I_o]$  CMD above the TRGB and at very red colors is populated by AGB stars and nothing else. It is obvious that RSG and AGB stars overlap in the red plume of a  $[(J-H)_o, H_o]$  CMD and that AGB stars are difficult to separate from RSG stars based on near-IR color. Using near-IR colors alone, on the other hand, we were able to identify a few additional, very red (in J-H) stars which were not seen in the optical. In Fig. 10, we coded the optically-identified AGB stars with black dots. We coded all stars found in the  $[(J-H)_o, H_o]$  CMD of VII Zw 403 which have a color  $>1.0$  and are above the TRGB with open circles. This illustrates the component of AGB stars found only in near-IR observations.

Mrk 178 is at a very similar distance as VII Zw 403. We transfer the above classification scheme to Mrk 178 in the following way. All stars with color  $< 0.5$  are shown in blue and are considered to be blue plume. Stars with colors  $0.5 < (J-H)_o < 0.85$  and H magnitude above the TRGB are shown as belonging to the red plume. Stars with colors above the TRGB are considered AGB stars, but only the “IR-detected ones in VII Zw 403” (colors  $> 1$ ) are emphasized with black dots, and the remaining objects are coded part of the red tangle.

Comparing the luminous stellar content of VII Zw 403 and Mrk 178, the most striking differences are the absence of very luminous RSGs and the presence of a very luminous BSG in Mrk 178. Small-number statistics could account for this. Another region where the two galaxies appear to differ is in the region between the two plumes. This could be an age effect — VII Zw 403 exhibits no W-R feature (Izotov 1998, private communication; Martin 1998, private communication) and could already be in a post-starburst phase. It could also be a metallicity effect — VII Zw 403 has a lower present-day gas metallicity. Assuming the stars are also of lower metallicity, we expect to see more blueward-extended blue loops in VII Zw 403.

There are a few very red stars at  $(J-H)_o \approx 1.5$  in both VII Zw 403 and Mrk 178. We verified that the red objects in Mrk 178 are indeed point-source-like in appearance. These stars can only be

some kind of long-period variable or very possibly, carbon stars. The near-IR observations of Feast et al. (1982) indicate that Mira stars tend to occur with  $(J-H)_o$  colors  $\approx 1.0$ . Colors redder than 1 mag, of up to about 1.2 mag, are preferentially seen in variable and non-variable stars of the S-type. The reddest colors, up to about 1.7 mag, are reached only by carbon stars. Spectroscopic follow-up observations are needed to unambiguously classify the very reddest stars in Mrk 178, but color selection based on near-IR colors has been one of the traditional and successful approaches to finding carbon stars in distant galaxies. While the ages of such stars are quite uncertain, their presence is usually taken as evidence for an intermediate-age population (Groenewegen 1999). Groenewegen & de Jong (1993) investigated the minimum mass for S and C-star formation in the LMC, and derived 1.5 and 1.2  $M_\odot$ , respectively. The lifetime of stars with these masses is about 2 and 4.25 Gyr in our  $Z=0.004$  grid. The detection of carbon stars therefore suggests that star-formation could have been active in Mrk 178 at ages earlier than the 1-2 Gyr frontier.

The question of the absence or presence of AGB stars has been of great importance for investigating the SFHs of dwarf elliptical (dE) and dwarf spheroidal (dSph) galaxies. In such galaxies the argument usually revolves around the detectability of low-mass stars in the E-AGB or TP-AGB phase. Low-mass stars, upon ascending the RGB for the second time, become brighter than the RGB tip in near solar-metallicity clusters (Frogel & Elias 1988; Guarnieri, Renzini & Ortolani 1997). In dwarf galaxies, with lower metallicity, this may not happen. Furthermore, in star-forming dwarfs there are so many AGB descendants of intermediate-mass stars clustering in the same region of the CMD that it is hard to distinguish the low-mass ones that would occur just above the TRGB. Age-dating using optical observations of AGB stars is also made difficult by the strong metallicity dependence of the isochrones. Theoretical models suggest that the near-IR tip-of-the-AGB magnitudes are much less dependent on metallicity, while retaining a strong age sensitivity (Bressan, Chiosi & Fagotto 1994). We can thus use the IR luminosity function of the stars above the TRGB to bracket the range of ages of the stellar population in Mrk 178. In Fig. 11 we show the H magnitude distribution of the AGB stars, defined as the objects redder than  $(J-H)_o=0.85$  and brighter than the TRGB, having adopted the “short” distance modulus of 28.1 so that  $M_{H_o,TRGB} = -5.5$ . The luminosity function is populated all the way up to  $M_{H_o} = -8.5$ , which translates into ages of a few hundred Myr in the Padova isochrones. Stellar generations with a wide range of ages overlap in this region of the CMD, and in principle could contribute to the luminosity function. (We are reluctant to use  $M_{H_o}$  as an indicator of  $M_{bol}$ . As discussed in SHGC99, the bolometric corrections are expected to depend on metallicity. If the reader so wishes, the transformation of Bessell & Wood (1984) may easily be applied to Fig. 11,  $M_{bol} = M_{H_o} + 2.6$ .) If we could unambiguously identify the low-mass AGB stars, then we would have an independent confirmation of star-forming activity taking place at ages which correspond to look-back times of several Gyr.

Let us now turn to the more luminous AGB stars. The descendants of intermediate-mass stars. Gallart et al. (1994) drew attention to the prominence of AGB stars in modern, CCD-based CMDs of star-forming galaxies. They noticed a very well-populated AGB red tail in the Local Group dwarf Irregular (dIrr) NGC 6822. According to stellar evolution models, a red tail with

extremely red colors in  $[(V-I)_o, I_o]$  CMDs occurs only at comparatively high metallicities. As the metallicity of the stellar models decreases, AGB stars become both bluer and brighter. Gallart et al. commented on the extremely red tail observed in NGC 6822, as well as in the LMC and the SMC, and suggested it be used to age-date stellar populations in such galaxies. An extended red tail appears in the  $[(V-I)_o, I_o]$  CMD of VII Zw 403, which presents somewhat of a puzzle (if we take the isochrones at face value) considering the low metallicity of the ionized gas (cf. SHCG99). As we pointed out repeatedly in our papers on VII Zw 403, stellar models are notoriously uncertain in the AGB phase, but having said that, we proceed with the comparison because otherwise there is little guidance as to the age of these stars. In Mrk 178, the red AGB population is less surprising; the metallicity of its ionized gas is high enough to support the presence of very red AGB stars.

We proceed to make a purely empirical comparison of the AGB populations in different star-forming galaxies. Our color selection criterion includes both E-AGB and TP-AGB stars. In Mrk 178, we find 56 sources redder than  $(J-H)_o$  of 0.85 of the total 791 (or about 7% of all stars detected). In VII Zw 403, we find 47 of 998 sources (or about 5% of stars detected) in this part of the near-IR CMD. Gallart et al. (1994) noted a 3% contribution of AGB stars to the observed, optical CMD of NGC 6822 (about 500 of 16300 sources). The selection effects of this CMD are different from the near-IR CMDs. Nevertheless the observations do make the point that modern CMDs are now routinely detecting AGB stars. Since the lifetimes of the E-AGB and especially the TP-AGB phases are short, a large number of progenitors is implied by the large number of such stars in the CMDs (cf. Renzini 1998). In other words, the luminous AGB stars require a parent population with ages of around a few hundred Myr and above. Thus, star-formation in Mrk 178 must have been active at times of around a few hundred Myr.

The near-IR CMD of Mrk 178 is populated by stars with a range of ages. We find young, massive stars in the blue plume; young, intermediate-mass AGB and possibly (intermediate-age?) carbon stars in the red plume; and older and lower-mass AGB and RGB stars in the red tangle. This evidence of star-formation across all “eras” of ages which are easily distinguishable with stellar indicators is very reminiscent of what we observed for VII Zw 403. In particular, our data do not show any obvious gaps in the stellar distribution (meaning, areas of the CMD which could, but are not, populated by stars). A gap in the distribution of stars is obvious in the CMD of the BCD I Zw 18. Fig. 7 of Aloisi, Tosi & Greggio (1999) shows a big gap in the red plume, between the region where one finds the brightest RSGs, and AGB/RGB stars; and it can be interpreted with a discontinuous SFH in recent (0.5 Gyr) times. In other words, I Zw 18 has undergone at least two episodes of star-formation separated by a distinct period of quiescence. The SFHs of Mrk 178 and VII Zw 403 are different. There are no such gaps in stellar distribution. These two galaxies are much closer than I Zw 18 (by about a factor of two or so); we would have noticed gaps. Rather, the CMDs of Mrk 178 and VII Zw 403 suggest a more-or-less continuous SFR, which was slightly elevated about 0.5 Gyr ago, and over a quite extended period of time.

## 4.2. Comparison with synthetic CMDs

In this section we provide synthetic CMDs for a variety of star-forming histories, and compare them with the Mrk 178 data. The advantage of using synthetic CMDs over a simple comparison of the data with isochrones or tracks is that the synthetic CMDs account for the lifetime in different stellar phases, and thus predict the relative numbers of stars across the CMD. With the help of synthetic CMDs we can also include, at least to some extent, the effects of measurement uncertainties and incompleteness. The synthetic CMDs presented here use the aforementioned stellar evolutionary tracks and stellar atmospheres, in a simulator presented for the first time by Tosi et al. (1991) and recently updated for use with HST WFPC2 data by Greggio et al. (1998). This code has now evolved to simulate NICMOS CMDs.

Basically, the code is used to calculate CMDs of composite stellar populations by random Monte Carlo extractions of stars, following an adopted initial mass function (IMF) and SFR law, including errors and incompleteness. On the observational side, while the errors and completeness functions were carefully investigated, uncertainties in the blending properties of stellar images and our distance calibration remain. The errors inherent to any given synthetic data point depend on how well a particular stellar evolution phase is presently understood. We note for instance that the simulations do not include the full TP-AGB phase, as the input tracks terminate at the first pulse. Other uncertainties include how well we can transform from the theoretical plane ( $M_{bol}$ ,  $T_{eff}$ ) to the observed plane (e.g.,  $M_H$ , J-H), the treatment of stellar atmospheres, and transformation to a given filter system. In addition, in modeling Mrk 178 it is not clear which metallicities are appropriate for the evolving stars. Finally, the distribution of errors at a given magnitude in the code does not match that for the data. In other words, the exact distribution of the data, including for instance such effects as outlying points outside of a Gaussian distribution, which will result from blending and near the detection limits, is not reproduced by our simulator. Although this will not affect our main conclusions, future versions of the code will need to model better the error distribution.

There are several free parameters that can be varied in order to achieve a match between the synthetic and the observed CMDs. Our data reach only the very top of the MS, which is poorly populated, making an IMF determination from the data impractical. More fundamentally, we should not derive an IMF from these data, because we are seeing only the Rayleigh-Jeans tail of their spectral energy distribution. Therefore, all simulations were carried out with the Salpeter IMF. The simulator includes stellar masses in the range from 0.6 to 120  $M_{\odot}$ , so the simulated SFRs and astrated masses refer to this mass range. It is easy enough to extend the mass range to lower masses, with any choice of low-mass IMF slope. In many papers on dwarf galaxies, one finds the use of the Salpeter IMF for the low-mass slope, and a low-mass cut-off of 0.1  $M_{\odot}$ . The mass range between 0.1 and 0.6  $M_{\odot}$  contributes 51% of the total stellar mass, although these low-mass stars are ten times as numerous as the more massive ones. We apply this correction factor to the total astrated mass.

Initially, we ran all simulations disregarding the fact that some stars on the CMD are located beyond the first thermal pulse on the tracks. The  $Z=0.0004$  simulations of Figure 12 are examples of these early simulations. To account for stars in the TP-AGB phase, we assumed that this phase lasts  $1.5 \times 10^6$  yr (Iben & Renzini 1983) and that they are produced in the  $1.5\text{--}3 M_{\odot}$  mass range. We chose the lower mass limit to approximate the minimum mass of carbon stars in the LMC. We first chose an upper limit of  $6 M_{\odot}$ , to approximate the minimum mass of stars which ignite non-violently. However, we found we were getting far too many stars in the TP-AGB region of the CMD. With an upper mass limit of 3 we still overproduce TP-AGB stars by up to a factor of two to three in some of the simulations. This problem is reminiscent of the missing bright AGB stars in the MCs (e.g. Frogel, Mould & Blanco 1990). Actually, the observed properties of intermediate age MC clusters and of field AGB stars now suggest that most of the TP-AGB stars originate from progenitors less massive than  $\approx 3 M_{\odot}$  (e.g., Marigo, Girardi & Chiosi 1996; Maraston 1998). In any case, the final CMDs (Fig. 13) show all “surviving” stars, minus those that would have been in this phase.

In Figure 12, we illustrate a sampling of synthetic CMDs for the two metallicities,  $Z=0.004$  and  $Z=0.0004$ , and the two distance scales, long and short, respectively. These CMDs show the surviving stars of a star-forming event that began 0.1, 2, or 15 Gyr ago and continued to the present epoch at a constant SFR. The  $Z=0.004$  simulations include the TP-AGB phase, while the  $Z=0.0004$  simulations were performed with the simulator before implementation of the TP-AGB counter. The SFHs adopted are quite simple, and provide basic insight into understanding the data. The synthetic CMDs also allow us to label each star according to its evolutionary phase. We note the several basic points.

First, Mrk 178 is clearly not a primeval galaxy. The synthetic CMDs which allow star-formation to occur only in the last 100 Myr are not populated with any stars in the red tangle.

Second, the  $Z=0.004$  grid gives a better description of the red colors of the luminous red stars than the  $Z=0.0004$  grid does. The low-metallicity models do not produce E-AGB stars of intermediate mass that are red enough to be consistent with the data, so for ages of up to several hundred Myr, the high-metallicity model is preferred. Hence, we suppose that the stellar metallicities of the young stars are indeed similar to that derived for the gas, at least in the sense that both clearly indicate a metallicity higher than  $Z=0.0004$  at the present epoch.

Third, a SFH extending up to 2 Gyr does not yield a distinctive TRGB feature in the  $Z=0.0004$  simulation. The synthetic CMD for  $Z=0.004$ , on the other hand, does have a feature that could be interpreted as a TRGB. However, it is at a lower luminosity than the “observed” TRGB. In this simulation, the linear branch of what we had observationally classed as RSGs in section 3, and the fan-shaped distribution of what we classed AGB stars, are well reproduced. In either of the two synthetic CMDs stars in the blue plume are overproduced.

Fourth, the synthetic CMDs which extend the SFH to 15 Gyr match better the small number of stars in the blue plume, and also present a distinct, TRGB feature. However, the red tangle is



too strong, and the number of luminous red stars above the TRGB is too small. In the  $Z=0.004$  synthetic CMD, the TRGB is most populated for J-H colors between about 0.9 and 1.2, whereas the TRGB in the data is most populated for J-H colors  $<0.9$ . Therefore, the  $Z=0.0004$  simulation provides for a better description of these data.

Evidently, the very simple SFHs adopted in these first attempts cannot match all the features of the data. From the previous discussion, better models would have a smaller number of stars in the blue plume and a distinct TRGB, while maintaining a linear RSG feature and a fan-shaped E-AGB/I component. To do this we constructed a SFH by considering separate regions in the CMD populated by stars born in different epochs. We selected three regions, which we'll briefly call the SG area, at magnitudes brighter than the TRGB and colors bluer than  $(J-H)_o=0.85$ ; the AGB area, in the same magnitude region, but at colors between 0.85 and 1; and the sub-TRGB area, defined as the region fainter than the TRGB. Comparison with the  $Z=0.004$  tracks (shifted by  $m-M=28.8$ ) shows that the SG area is basically populated only by massive stars, thus sampling the SF during the last 100 Myr; the AGB area mostly ages between 100 Myr and 1 Gyr; the remaining portion of the CMD samples the epochs older than this. We ran distinct simulations for the three regions. The first two were constrained to reproduce the observed number of objects in the SG and AGB areas, with stars born in the appropriate age ranges. Each of these simulations brings along synthetic objects falling in the the sub-TRGB area, according to the stellar evolution prescriptions. The remaining objects observed in the sub-TRGB area were then produced by running a third simulation with star formation episodes older than 1 Gyr. One model is obviously composed of the sum of the three simulations. We notice that we did not try to correct for simulated TP-AGB stars, due to the theoretical uncertainty affecting their lifetimes and mass range.

We considered two cases for the metallicity:  $Z=0.004$  with the corresponding distance modulus of 28.8, and a mixed-metallicity case, in which the RGB stars have  $Z=0.0004$ , and the remaining, younger stars have  $Z=0.004$ . Since the distance is derived from the TRGB, the assumed distance modulus in the mixed- $Z$  simulation is 28.1. With the short modulus, the evolutionary masses sampled by the SG and AGB areas are lower than described above, and correspond to different age bins. In the mixed case we used ages up to 400 Myr, and from 400 Myr to 1 Gyr, for the SG and AGB areas, respectively. In principle, the entire age range from 1 to 15 Gyr is available for the third simulation, which had to produce typically 200 stars in the  $Z=0.004$  case, 350 in the mixed metallicity case. In practice, the distribution of stars very poorly constrains this age range. We explored various options for the old SF, on which we comment below.

The numbers of observed stars in the SG and in the AGB areas, which constrain the relative simulations, are small (a few tens). To model statistical effects, we ran simulations in which we allowed the constraints to vary by the RMS of the number of stars actually present in the observed CMD. In Fig. 13 we show two exemplary synthetic CMDs (with the oldest episode spanning the whole 1-15 Gyr range), together with the data. The simulator does not produce the few sparse objects at the reddest J-H colors. At bright magnitudes, the reddest stars are TP-AGB objects, counted by the simulator, but not placed on the CMD. At faint magnitudes the simulator does not

reproduce the error distribution to a great accuracy. A better description of this would certainly improve the appearance of the synthetic CMDs, but hardly change our basic conclusions.

The salient features of the simulations shown in Fig. 13 are the following. For the high metallicity simulation, the SFR (corrected to extend the IMF down to  $0.1 M_{\odot}$ ) is  $2.6 \times 10^{-3} M_{\odot} \text{ yr}^{-1}$  in the last 100 Myr,  $5.5 \times 10^{-3} M_{\odot} \text{ yr}^{-1}$  from 1 Gyr to 100 Myr ago, and  $4.3 \times 10^{-4} M_{\odot} \text{ yr}^{-1}$  from 15 to 1 Gyr ago. This drop comes about because this is an average SFR over a long period of time. The set of models of this kind yield a SFR ranging between 2.6 and  $3.7 \times 10^{-3} M_{\odot} \text{ yr}^{-1}$  in the young component; between 5.5 and  $6.8 \times 10^{-3} M_{\odot} \text{ yr}^{-1}$  in the intermediate age component. These simulations also produce between 159 and 187 TP-AGB stars beyond the end of our tracks: too many, as stated above.

For the mixed-metallicity simulation, the age bins are 0 to 400 Myr, 400 Myr to 1 Gyr, and 1 to 15 Gyr. For the youngest ages, the SFR derived is between 0.9 and  $1.3 \times 10^{-3} M_{\odot} \text{ yr}^{-1}$ . These values are somewhat low compared to the spectroscopically derived rate of  $>3 \times 10^{-3} M_{\odot} \text{ yr}^{-1}$ ; however, they also cover a clearly longer time-interval than the one probed by the  $H_{\alpha}$  emission. (We show the case of the highest SFR in Fig. 13.) For the intermediate ages, the SFRs we obtain are between 2.0 and  $7.0 \times 10^{-3} M_{\odot} \text{ yr}^{-1}$ . (We show our case of  $3.5 \times 10^{-3} M_{\odot} \text{ yr}^{-1}$ .) The number of TP-AGB stars produced is between 60 and 173, less of an overproduction than in the previous set of simulations. For the oldest stars, the average SFR over this long time interval drops to  $4.5 \times 10^{-4} M_{\odot} \text{ yr}^{-1}$ .

What can we take away as secure results from these simulations? Fig. 13 indicates that both simulations reproduce well the blue plume and the RSG “finger” of the observed CMD. It appears that the SFR of Mrk 178 in the last few 10 Myr has been of the order of a few times  $10^{-3} M_{\odot} \text{ yr}^{-1}$ . This answer comes from both the  $H_{\alpha}$  luminosity, and the simulations of the supergiant stellar content of the CMD. Both simulations also produce a stubby, luminous AGB “finger” with J-H colors redder than 0.85. It is here that we expect only a crude qualitative match, since we are missing the TP-AGB phase in the synthetic CMDs. As we go back to ages of around about 0.5 Gyr, the SFR seems to have been slightly higher. Both sets of simulations give SFRs that are up by a factor of a few (2 to 5) in this era of the galaxy’s history as compared to more recent times. For ages upward of 1 Gyr, the SFRs that come out of the two sets of simulations are very similar. To compare the simulations with the data, note that in the data, the red edge of the red tangle is at a J-H color of 0.9. Beyond a color of 0.9, the stellar numbers drop off; it is here that we also get the data with the highest error bars, which are not captured well by the simulations. The simulation with  $Z=0.004$  produces a red tangle which is clearly too red. It has the morphological appearance of a third, RGB “finger”, which sticks out of the red tangle at a slant. The  $Z=0.0004$  red tangle does not exhibit this morphology. It reproduces well the overall, triangular shape of the red tangle in the data. However, the red edge in this red tangle is too blue by about 0.1 mag, giving the appearance of too many stars in the red tangle. We have a slight preference for a predominantly low-metallicity RGB, because it yields a red tangle that is located beneath the luminous portion of the red plume, a “sharp” red edge for the red tangle, and an overall distribution of stars near the

TRGB which reproduces the data quite well.

We now describe our efforts to set some limits on the SFH of Mrk 178 beyond the age of 1 Gyr. Our first argument is based on the total mass in stars. We derived the SFR over a certain time interval, so multiplying the SFR with this time interval yields the total astrated mass encompassed by the NIC2 field. Since the NIC2 field was located near the center of Mrk 178, let us assume the mass we derive is representative of a good fraction of the galaxy’s mass. Stars that populate the red tangle, in particular those in the oldest of our age bins, strongly influence our result concerning the early star-formation in Mrk 178 and thus, its total astrated mass. It is possible to find good matches of the observed CMD for a variety of fractional contributions of intermediate versus low-mass stars to the red tangle. If more of the red tangle is thought to arise from higher mass stars, the total astrated mass is lower. The lowest total astrated masses consistent with our data are from models which constrict the SF to the 1 to 2 Gyr age range.

For example, if we add in the high-metallicity simulation the 200 stars in the RGB area over the age interval of 1 to 15 Gyr (as was done in the exemplary simulation discussed above), they are drawn from a population with a total mass of about  $6 \times 10^6 M_{\odot}$ . The same is true if we add over this time interval the 350 RGB stars of low-metallicity (since the average SFRs of the two cases simulated are so similar). If instead we add them only over an age range of 1 to 2 Gyr, then the total mass drops down to about  $3 \times 10^6 M_{\odot}$ . Finally, if for instance we add these stars between 14 and 15 Gyr, then the mass goes up to just over  $1 \times 10^7 M_{\odot}$ . Thus, while in general both the time and duration of low-mass star formation control the mass of the galaxy, we find that a short event early on in the history of the galaxy produces a higher mass than long-term, low-level star-forming activity, and a short event late in the history of the galaxy.

We have little guidance concerning the amount of mass we really should expect to be locked up in stars. Observed masses for BCDs usually are for the neutral gas (H-I) content, or some dynamical mass that includes the dark matter. The blue luminosity derived in section 3.2 cannot be used, as it is dominated by the young stars with a very different mass-to-light ratio than that of the old stars. Nonetheless, note that the highest astrated mass can be achieved by adding most stars early in the galaxy’s life, and that the total mass in stars can in this way be raised to be of the order of  $10^7 M_{\odot}$ . This is of the same order of magnitude as the H-I mass of Mrk 178. If, on the other hand, we assume that this galaxy is no older than 2 Gyr, in other words, if we assume all of the stars were added just at the 1-2 Gyr frontier, then the total astrated mass is only a few times  $10^6 M_{\odot}$ . While the differences are not dramatic (a factor of three or so), one wonders whether the stellar mass of a BCD is comparable to the mass of a very massive globular cluster like  $\omega$  Cen (Pryor & Meylan 1993), or whether it should instead be significantly higher. Unfortunately we cannot be sure how much mass is contained in the background sheet discussed in the next section. As Fig. 1 indicates, the NIC2 field was located near the bright central regions of the elliptical light distribution, which we assume to dominate the galaxy’s mass. If the stars in the background sheet contribute a few (as in, up to 10) times the mass encompassed by the NIC2 field, then our guesses for the stellar mass independently of the exact formation age are of the order of  $10^7$ - $10^8 M_{\odot}$ .

The determination of galaxy masses is one of the potential strengths of CMD studies, but to accomplish this, the CMDs need to be deep enough to reveal directly the low-mass stars. Once the SFR at all ages is determined, it can in principle be integrated to derive a value for the total mass. This is already being done for Local Group dwarfs. For the more distant BCDs, this will perhaps become feasible observationally for a few nearby examples with the NGST. Suffice it to say that the hypothesis of Izotov & Thuan, in which BCDs are either primeval for extremely low metallicities, or no older than 1-2 Gyr in the case of low metallicities, goes hand in hand with saying that these galaxies have low astrated masses.

Our second argument addresses the question whether or not Mrk 178 could be a faint blue galaxy. Following the hypothesis of Babul & Ferguson (1996), the faint blue galaxies are small, low-mass galaxies that undergo very short ( $10^7$  yr) starbursts at redshifts of about 0.5 to 1. The number of stars in the red tangle now is used to constrain the burst strength. The SFRs in the simulations of the 1-2 Gyr or 14-15 Gyr events in Mrk 178 are not high, of the order of several times  $10^{-3}M_{\odot}\text{yr}^{-1}$ . Therefore, a Gyr-long SF event would not be able to generate the SFR needed in the Babul & Ferguson model; it falls short by several orders of magnitude. Even a short (0.1 Gyr) burst at intermediate (5 or 7.5 Gyr) age can bring the SFR up to only a few times  $10^{-2}M_{\odot}\text{yr}^{-1}$ , and still falls short of the  $1-10 M_{\odot}\text{yr}^{-1}$  assumed in the Babul & Ferguson scenario. An extremely short, 10 Myr starburst, between 7.5 and 15 Gyr, matching pretty closely the input parameters of the Babul & Ferguson models, raises the SFR to  $0.6-1 M_{\odot}\text{yr}^{-1}$ ; this is approaching the order-of-magnitude SFR required. In other words, it is *possible* that the red tangle of Mrk 178 hides an event that is consistent with that required to call it a faint blue galaxy. However, to accomplish this the galaxy had to form over an extremely short time period and at early times, as well as remain inactive until the onset of the recent SF activity.

In summary, the CMD simulations have given us the following insights into the SFH of Mrk 178. As in VII Zw 403 (cf. Lynds et al. 1998), the SFR seems to have been higher about a few hundred Myr ago, then it was in the more recent past. The CMD requires that stars formed more than 1 Gyr ago — and the older the stars, the better defined the TRGB and the higher the astrated mass. A very short burst of star formation at an early epoch can be hidden in the data; Mrk 178 could be a descendent of the Faint Blue Excess population of galaxies in deep images.

### 4.3. Morphology

Loose & Thuan (1986) performed a deep CCD imaging survey of 50 BCDs from the list of Thuan & Martin (1981). They found that over 95% of BCDs show red halos of light which extend beyond the star-forming regions and which suggest the presence of an old, underlying stellar population. These galaxies are the best candidates among the BCDs for harboring dynamically relaxed, old stellar substrata. Conversely, the question of whether or not the remaining few objects for which such regular, extended outer isophotes have not been discovered are primeval galaxies remains a matter of great interest (e.g. Izotov & Thuan 1999, SHCG99).

In the case of VII Zw 403, we were able to demonstrate that the RGB population not only underlies the centrally located star-forming region, but is the dominant population at large galactocentric radii. Previously, the red color derived from spatially integrated surface photometry of the halos of BCDs was used to infer the presence of an ancient background sheet of stars (e.g. Loose & Thuan 1986, Kunth, Maurogordato & Vigroux 1988, Papaderos et al. 1996, Telles, Melnick & Terlevich 1997, Meurer 1999). However, RGB, AGB and RSG stars overlap in temperature, and hence color. The direct detection of individual RGB stars far from the center of VII Zw 403 (SHCG99) provided the necessary evidence that the integrated red colors may indeed be due to RGB stars and thus a stellar population that is significantly older than the starburst.

For Mrk 178, we detect an RGB substratum in the inner regions of the galaxy, but we have no resolved stellar photometry for the halo. The DSS image (Fig. 1) and available CCD images, however, testify to the presence of extended outer isophotes with regular, elliptical contours. To emphasize this point, we show in Fig. 14 a slightly manipulated version of the DSS image. We performed a sky subtraction and smoothing with a 3-pixel ( $\approx 5''$ ) boxcar filter, and show the result as a contour plot. From this plot we infer that the major axis may be traced to at least  $2'$ , much further out than the size listed in the RC3 ( $1/23$  to the standard, 25-magnitude level). This illustrates that indeed a very faint and very extended background sheet exists. The stars populating the extended halo contribute to the total mass of the galaxy, but with the data in hand, we cannot derive a reasonable estimate of how much.

There are no surface-brightness profiles available for Mrk 178. Huchra (1977) gives aperture photometry in a series of increasing circular apertures. In Table 1, we reproduce colors in the smallest aperture, which happens to coincide closely with the size of the NIC2 field, and in two rings of increasing size. According to Table 1, the colors are bluest, in the smallest,  $24''$  measurement aperture, and rise to an intermediate color in the  $24''$ - $56''$  ring and the  $38''$ - $56''$  ring. The data thus suggest that Mrk 178 becomes redder outside of the star-forming core. This is the behavior generally observed for type iE BCDs.

We compared the aperture photometry of Mrk 178 with the integrated, empirical star-cluster colors of Schmidt, Alloin & Bica (1995). Schmidt, Alloin & Bica derived these data using as spectral templates young and intermediate-age clusters in the SMC, LMC and Galaxy disk. Their dwarf Elliptical/dwarf Spheroidal (dES) galaxy template is constructed using spectral libraries of three metal-poor galactic globular clusters. No U-V colors are available in the Schmidt, Alloin & Bica database. The observed colors of Mrk 178 were overlaid onto their Fig. 9 diagnostic diagram. It is evident that the color in the smallest aperture is consistent with that of the youngest cluster templates in the age range from 20 Myr to 200 Myr. The colors in the rings, on the other hand, can be matched by clusters with ages of 200 to 700 Myr.

We interpret the color at radii beyond the NIC2 field as follows. Young stars are the dominant population in the core where the NIC2 field was located; they outshine any older stars in integrated light. The young, blue stars are concentrated near the center, in the two prominent H-II regions.

This component to the integrated light decreases away from the core of the galaxy toward its halo, so that the older stars become a more important contribution to the integrated light at larger radii. This is reminiscent of the core-halo structure seen in the resolved stars in VII Zw 403 (SHCG99).

To summarize, Mrk 178 exhibits the same iE morphology as VII Zw 403, the most common type in the Loose & Thuan sample. We have now demonstrated the existence of RGB stars in two such BCDs. This supports the hypothesis put forth based on the morphology and the colors of the red halos of BCDs (Loose & Thuan 1986, Kunth, Maurogordato & Vigroux 1988, Papaderos et al. 1996, Telles, Melnick & Terlevich 1997, Meurer 1999) that all BCDs with extended, red background sheets harbor old stars.

## 5. Conclusions

Mrk 178 is a typical BCD in terms of its morphology, size, luminosity, H-I mass, and gas abundances. In its H-II regions, its star-formation rate is at least a few times  $10^{-3}M_{\odot}\text{yr}^{-1}$ . This is typical for the SFR of a late-type dwarf.

We use near-IR photometry with the HST to find the RGB, showing that Mrk 178 must be at least 1-2 Gyr old. The older this population the better it fits at the TRGB, and the higher the total astrated mass of the galaxy. Employing a calibration previously derived by us for the TRGB method in the near-IR, we determine a minimum distance of  $4.2(\pm 0.5)$  Mpc for Mrk 178. This distance is 17% larger than that based on ground-based photometry of the brightest resolved objects. In applying the near-IR TRGB method for the first time to a galaxy for which there is no optical TRGB, we encountered several problems. First, lacking a metallicity calibration for the RGB in the near-IR, the distance estimate assumes that  $-2.3 < [\text{Fe}/\text{H}] < -1.5$  for old RGB stars. A higher metallicity has the effect of increasing the distance. Second, Mrk 178 exhibits a very strong AGB component. These stars have similar colors as RGB stars and luminosities that extend above the TRGB. Their effect is to add noise to the luminosity functions from which we are attempting to determine the onset of the TRGB feature. This is an obvious drawback of the near-IR TRGB method.

Luminous AGB stars account for as much as 7% of the resolved stars in our CMD, and populate a distinct area in color and luminosity space. Their presence indicates that star-formation was active and strong several hundred Myr ago. The upper limit to the age of the stars in the AGB area brighter than the TRGB is difficult to establish, since tracks of a wide range of initial masses overlap in this region. There may even be a contribution from stars as old as several Gyr, as inferred for early-type dwarfs.

We find several objects with extremely red near-IR colors and suggest that they are carbon stars. The detection of candidate carbon stars in BCDs is a result which only became possible with the advent of deep near-IR photometry.

We use Monte-Carlo simulations to constrain the SFH quantitatively. For stellar ages below 1 Gyr, the observed CMD provides good constraints on the SFH. The prominent red-tangle feature potentially contains truly ancient stars. Synthetic CMDs with a range of SFHs all produce reasonably matching red tangles. However, when the red tangle is attributed exclusively to relatively young stars with ages between 1 and 2 Gyr, then the total astrated mass of the galaxy (within the NICMOS field-of-view) is as small as that of a massive globular cluster. The further the SF extends to earlier ages, the higher the total astrated mass.

In order to explore whether or not Mrk 178 could be the descendant of a faint blue galaxy, we modeled the SFH beyond 1 Gyr with short bursts. The total number of available stellar progeny of an intermediate-age burst in the red tangle limits the possible burst strength. Assuming a burst duration of 10 Myr, such a potential burst was of the right order of magnitude in strength compared to what is needed in the Babul & Ferguson (1996) scenario.

The main question we set out to answer was whether Mrk 178 is young or old. While our CMDs alone cannot prove the existence of RGB stars older than a few Gyr, we argue that the detection of RGB stars in combination with the morphology of Mrk 178 provides a strong indication for the presence of low-mass stars and hence, a large formation age of this galaxy.

Work on this project was supported through HST grants to RSL and MMC (projects 7859 and 8012). UH acknowledges financial support from SFB 375. We thank Quentin Bailey for writing a piece of code that allowed RSL to compare luminosity functions. We also thank Dr. Deidre Hunter for sharing her unpublished data. We made extensive use of the SIMBAD and NED data bases.

NOTE ADDED IN PROOF: After this paper was accepted, we learned that in February of 2000, P. Papaderos of the University of Göttingen obtained deep, ground-based CCD images of Mrk 178 at the Calar Alto 1.23-m telescope. He communicates to us that his images in the Johnson-Cousins B and R system clearly exhibit an extended red sheet which is very faint, regular, and elliptical in shape; he also identifies about 20 faint star-forming regions in the north-eastern parts of the galaxy which were not encompassed by the NIC2 FOV. The color profile shows that outside of 30–35'' (well outside of the central, dominant H-II regions at which we pointed the NIC2) Mrk 178 becomes quite red,  $(B-R)_0 \approx (1.1 \pm 0.1)$  mag, supporting the idea that this is not a young galaxy.

## REFERENCES

- Aloisi, A., Tosi, M., Greggio, L. 1999, *AJ*, 118, 302  
Bertelli, G., Bressan, A., Chiosi, C., Fagotto, F., Nasi, F. 1994 *A&AS*, 106, 275  
Bessell, M.S., Castelli, F., Plez, B. 1998, *A&A*, 333, 231  
Bessell, M.S., Wood, P.R. 1984, *PASP*, 96, 247

- Bressan A., Chiosi, C., Fagotto, F. 1994, ApJS, 94, 63
- Burstein, D., Heiles, C., 1984, ApJS, 54, 33
- Da Costa, G.S., 1994, in “Third CTIO/ESO Workshop on The Local Group: Comparative and Global Properties”, ed. A. Layden, R. C. Smith, J. Storm (Munich: ESO), 101
- Dekel, A., Silk, J., 1986, ApJ, 303, 39
- Ellis, R.S. 1997, ARA&A, 35, 389
- Fagotto, F., Bressan, A., Bertelli, G., Chiosi, C. 1994, A&AS, 104, 365
- Feast, M.W., Robertson, B.S.C., Catchpole, R.M., Lloyd Evans, T., Glass, I.S., Carter, B.S. 1982, MNRAS, 201, 439
- Ferguson, H.C., Babul, A. 1998, MNRAS, 296, 585
- Ferrara, A., Tolstoy, E. 2000, MNRAS, 313, 291
- Frogel, J.A., Elias, J.H. 1988, ApJ, 324, 822
- Frogel, J.A., Mould, J., Blanco, V.M. 1990, ApJ, 352, 96
- Gallart, C.; Aparicio, A.; Chiosi, C.; Bertelli, G.; Vílchez, J.M. 1994, ApJ, 425, L9
- Georgiev, Ts. B., Karachentsev, I.O., Tikhonov, N.A. 1997, AstL, 23, 514
- González-Riestra, R., Rego, M., Zamorano, J. 1988, A&A, 202, 27
- Greggio, L. 1986, A&A, 160, 111
- Greggio, L., Tosi, M., Clampin, M., De Marchi, G., Leitherer, C., Nota, A., Sirianni, M. 1998, ApJ, 504, 725
- Groenewegen, M.A.T. 1999, in “Asymptotic Giant Branch Stars”, ed. T. Le Bertre, A. Lèbre, and C. Waelkens (IAU Symp. 191: ASP), 535
- Groenewegen, M.A.T., de Jong, T 1993, A&A, 267, 410
- Guarnieri, M.D., Renzini, A., Ortolani, S. 1997, ApJ, 477, L21
- Guzmán, R., Jangren, A., Koo, D.S., Bershadsky, M.A., Simard, L. 1998, ApJL, 495, 13
- Huchra, J.P. 1977, ApJS, 35, 171
- Huchtmeier, W.K., Hopp, U., Kuhn, B. 1997, A&A, 319, 67
- Hunter, D. A., Gallagher, J. S. 1986, PASP, 98, 5
- Hunter, D. A. 2000, in preparation
- Iben, I., Renzini, A. 1983, A&AR, 21, 271
- Ikeuchi, S., Norman, C. 1987, ApJ, 312, 485
- Izotov, Y.I., Thuan, T.X. 1999, ApJ, 511, 639
- Kobulnicky, H.A., Skillman, E.D. 1996, ApJ, 471, 211



- Koo, D. C., Bershad, M. A., Wirth, G. D., Stanford, S. A., Majewski, S. R. 1994, *ApJ*, 427, L9
- Koo, D.C., Guzmán, R., Faber, S.M., Illingworth, G.D., Bershad, M.A., Kron, R.G., Takamina, M. 1995, *ApJ*, 440, L49
- Kunth, D., Maurogordato, S., Vigroux, L. 1988, *A&A*, 204, 10
- Lee, M.G., Freedman, W.L., Madore, B.F., 1993, *ApJ*, 417, 553
- Loose, H.H., Thuan, T.X. 1986, in *Star-Forming Dwarf Galaxies and Related Objects*, ed. D. Kunth, T.X. Thuan, and J. Tran Than Van (Gif-sur-Yvette: Éditions Frontières), 73
- Lynds, R., Tolstoy, E., O’Neil Jr., E.J., Hunter, D.A. 1998, *AJ*, 116, 146
- Maeder, A., Conti, P.S. 1994, *ARA&A*, 32, 227
- Maraston, C. 1998, *MNRAS*, 300, 872
- Marigo, P., Girardi, L., Chiosi, C. 1996. *A&A*, 316, L1
- Marzke, R.O., Da Costa, L.N. 1997, *AJ*, 113, 185
- Meurer, G.R. 1999, in “Dwarf Galaxies and Cosmology”, ed. T.X. Thuan, C. Balkowski, V. Cayatte, and J. Tran Than Van (Gif-sur-Yvette: Éditions Frontières), 337
- Papaderos, P., Loose, H.-H., Thuan, T.X., Fricke, K.J. 1996, *A&AS*, 120, 207
- Popescu, C.C., Hopp, U., Rosa, M.R. 1999, *A&A*, 350, 414
- Pryor, C., Meylan, G. 1993, in *ASP Conference Series*, 50, 193
- Renzini, A. 1998, *AJ*, 115, 2459
- Schlegel, D.J., Finkbeiner, D.P., Davis, M. 1998, *ApJ*, 500, 525
- Schmidt, A.A., Alloin, D., Bica, E. 1995, *MNRAS*, 273, 945
- Schulte-Ladbeck, R.E., Crone, M.M., Hopp, U. 1998, *ApJ*, 493, L23 (SCH98)
- Schulte-Ladbeck, R.E., Hopp, U. 1998, *AJ*, 116, 2886
- Schulte-Ladbeck, R.E., Hopp, U., Crone, M.M. Greggio, L. 1999, *ApJ*, 525, 709 (SHCG99)
- Schulte-Ladbeck, R.E., Hopp, U., Greggio, L., Crone, M.M. 1999, *AJ*, 118, 2705 (SHGC99)
- Searle, L., Sargent, W.L.W. 1972, *ApJ*, 173, 25
- Searle, L., Sargent, W.L.W., Bagnuolo, W.G. 1973, *ApJ*, 179, 426
- Skillman, E.D., Bender, R., 1995, *RevMexAA*, 3, 25
- Skillman, E.D. , Dohm-Palmer, R.C., Kobulnicky, H.A. 1998, in *Bonn/Bochum-Graduiertenkolleg Workshop*, ed. T. Richtler & J.M. Braun (Shaker Verlag), 77
- Stetson, P.B., Davis, L.E., Crabtree, D.B. 1990, in *ASP Conf. Proc. 8, CCDs in Astronomy*, ed. G.H. Jacoby (San Francisco:ASP), 289
- Sweigart A.V., Greggio, L., Renzini A. 1990, *ApJ*, 364, 527
- Telles, E., Melnick, J., Terlevich, R. 1997, *MNRAS*, 288, 78

- Thuan, T.X., 1991, in “Massive Stars in Starbursts”, ed. C. Leitherer, N.R. Walborn, T.M. Heckman, & C.A. Norman (Cambridge: Cambridge Univ. Press), 183
- Thuan, T.X., Martin, G.E. 1981, ApJ, 247, 823
- Tosi, M., Greggio, L., Marconi, G., Focardi, P. 1991, AJ, 202, 951
- White, S.D.M., Rees, M.J. 1978, MNRAS, 183, 341

Fig. 1.— The 4'x4' 103a-E image of Mrk 178 from the Digitized Sky Survey in grey-scale representation. The brightest feature is a blend of the two main H-II complexes. This is where the NIC2 camera was pointed. The faint, elliptical main body can also be seen.

Fig. 2.— NIC2 color image composed from combining the images taken through the F110W and F160W filters. This image is about 19" x 19".

Fig. 3.— The DAOPHOT-derived photometric errors.

Fig. 4.— Completeness fractions from ADDSTAR tests.

Fig. 5.— Color-magnitude diagrams of Mrk 178 in magnitudes in the HST Vega system. The location of the TRGB is indicated. The luminosity function in F110W (see Fig. 6) exhibits a sharp jump; this is where we mark the TRGB in the upper panel. The luminosity function in F160W displays a gradual rise; this is due to the slanted TRGB in the bottom panel (where our estimated errors are indicated by dashed red lines).

Fig. 6.— Luminosity functions of Mrk 178 in magnitudes in the HST Vega system for stars with  $0.75 < (F110W-F160W) < 1.5$ . The location of the TRGB is indicated. Notice the high completeness at the TRGB. We can also see the contribution to the luminosity functions by AGB stars at magnitudes brighter than the TRGB.

Fig. 7.— Color-magnitude diagrams of Mrk 178 after transformation to ground-based J and H. The foreground extinction is negligible.

Fig. 8.— Color-magnitude diagrams of Mrk 178 with three cuts applied on the size of the photometric errors ( $1\sigma$ ) in both J and H. The salient features of Fig. 7 remain when only data with good errors are being considered. Notice by comparison with Fig. 7 or 9 that many faint and very red, and some faint and blue stars, have large errors.

Fig. 9.— Color-magnitude diagrams of Mrk 178 with two sets of tracks overlaid. The first set of tracks is for a metallicity of  $Z=0.0004$  and the corresponding short distance modulus of 28.1. The second set is for  $Z=0.004$  and the long distance modulus of 28.8. For each case, the TRGB is indicated, and the corresponding absolute-magnitude scale is given on the right-hand ordinate.

Fig. 10.— A comparison of the near-IR CMDs of VII Zw 403 and Mrk 178. The data for Mrk 178 are selected to have J and H errors smaller than 0.2 mag. The color-coding is blue for MS, BSG, and BL stars; magenta for RSG and luminous AGB stars; red for RGB and faint AGB stars; black for AGB stars; with black circles (in the case of VII Zw 403) and large black dots (in the case of Mrk 178) for near-IR identified AGB stars (presumably in the TP-AGB phase). For more details, refer to the text. The TRGB is shown by dashed green lines. The dashed blue lines indicates the location of the blue plume. The dashed red line indicates where more stars might belong to the RGB phase in Mrk 178 and the black dashed line indicates where optically-identified AGB stars are separable from RSGs in the VII Zw 403 CMD.

Fig. 11.— The number of AGB stars detected in the near-IR as a function of their luminosity in Mrk 178 and VII Zw 403. Stars just above the TRGB, at around  $M_H=-6$ , could be low-mass and hence old, AGB stars (see text).

Fig. 12.— Synthetic CMDs for  $Z=0.0004$  (left) and  $Z=0.004$  (right), using the Salpeter IMF, the appropriate distance, and a constant SFR, in the interval from the maximum time indicated in each panel to the present epoch. The simulator for  $Z=0.0004$  did not have the TP-AGB counter enabled, so all survivors are plotted. The  $Z=0.004$  simulator shows all survivors minus the TP-AGB stars, for which we do not have tracks or atmospheres. The dashed lines drawn indicate the observed location of the TRGB, the center of the blue plume, and the “dividing line” of the RSG vs. (optically detected) AGB stars.

Fig. 13.— A comparison of the data with two exemplary, synthetic CMDs. For these complex SFHs, the history of the galaxy was divided into 3 age bins. The simulation labeled “ $Z=0.004$ ” uses high-metallicity models and assumes the long distance scale. The simulation labeled “ $Z$  mixed” uses  $Z=0.0004$  for stars with ages greater than 1 Gyr and  $Z=0.004$  for younger stars, and assumes the short distance scale.

Fig. 14.— A contour-plot of the DSS image, after sky subtraction and smoothing with a 3-pixel ( $\approx 5''$ ) boxcar filter. This representation shows very well the large extent of the faint, elliptical halo, and emphasizes the type “iE” morphology of Mrk 178.

This figure "sl\_mrk\_fig1.gif" is available in "gif" format from:

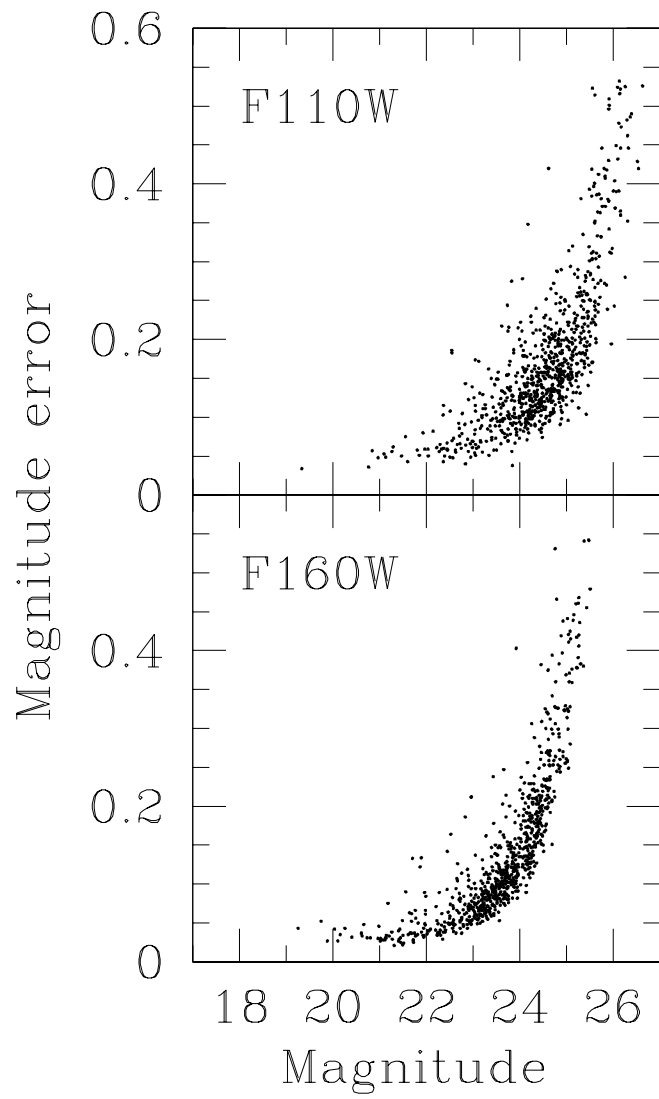
<http://arxiv.org/ps/astro-ph/0007417v1>

Table 1. APERTURE PHOTOMETRY OF MRK 178

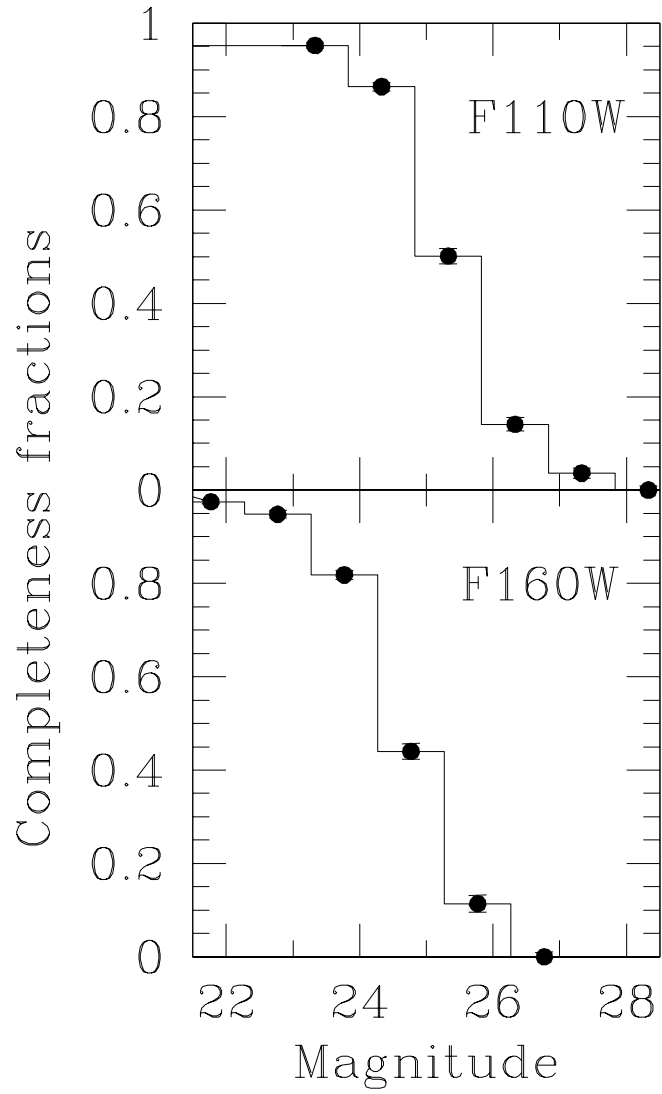
Aperture	$\leq 24''$	24''-56''	38''-56''
U-V	-0.26	0.43	0.60
B-V	0.27	0.45	0.44
V-R	0.34	0.51	0.44

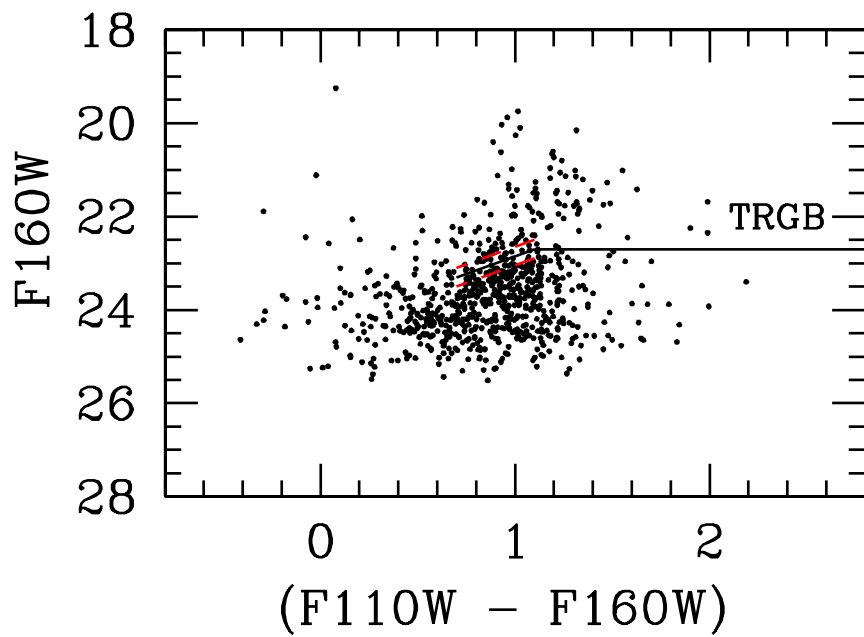
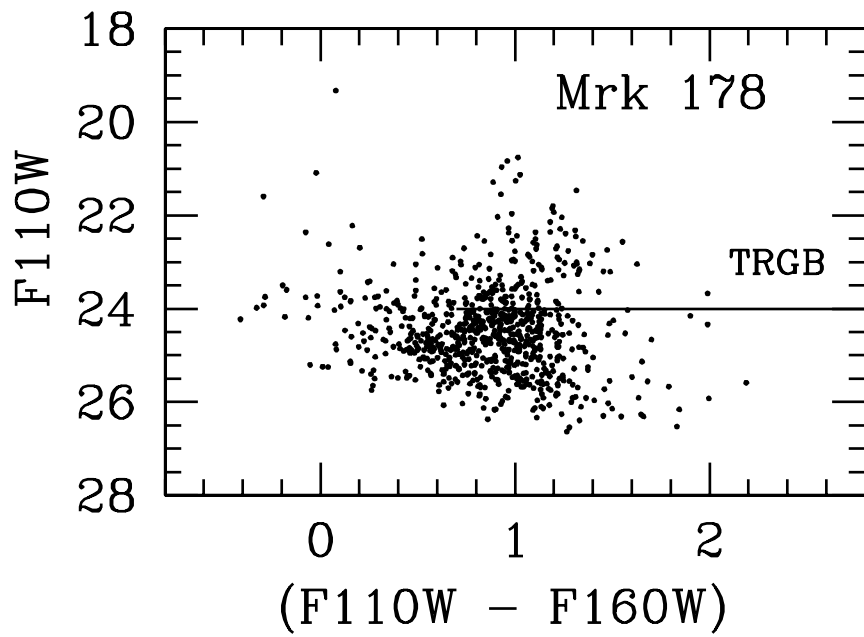
This figure "sl\_mrk\_fig2.gif" is available in "gif" format from:

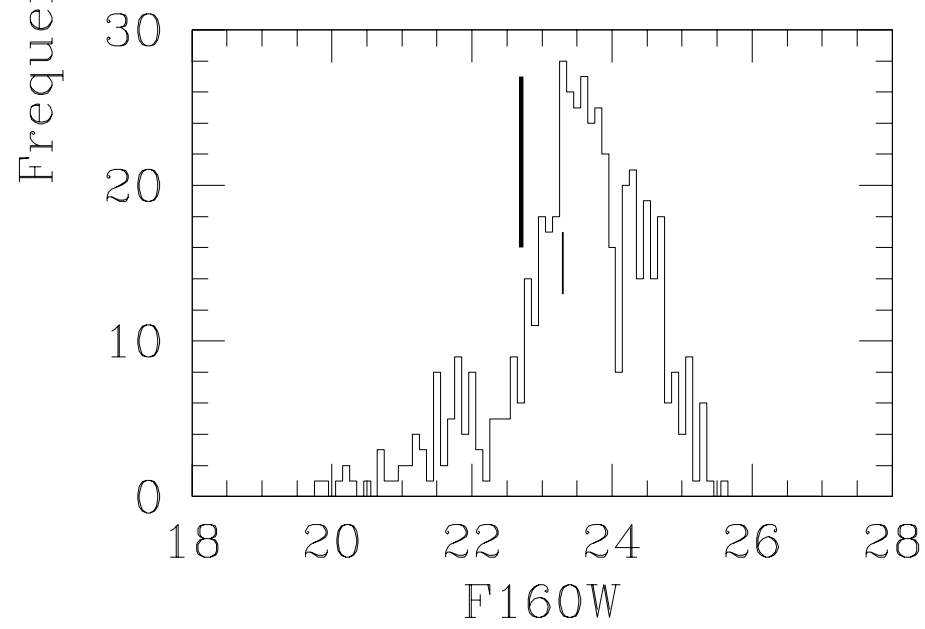
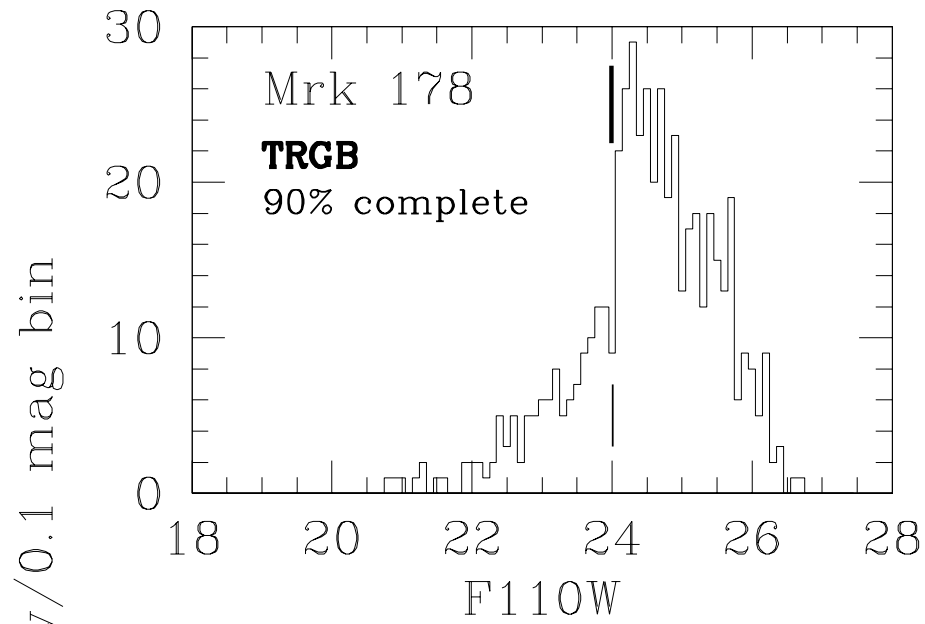
<http://arxiv.org/ps/astro-ph/0007417v1>

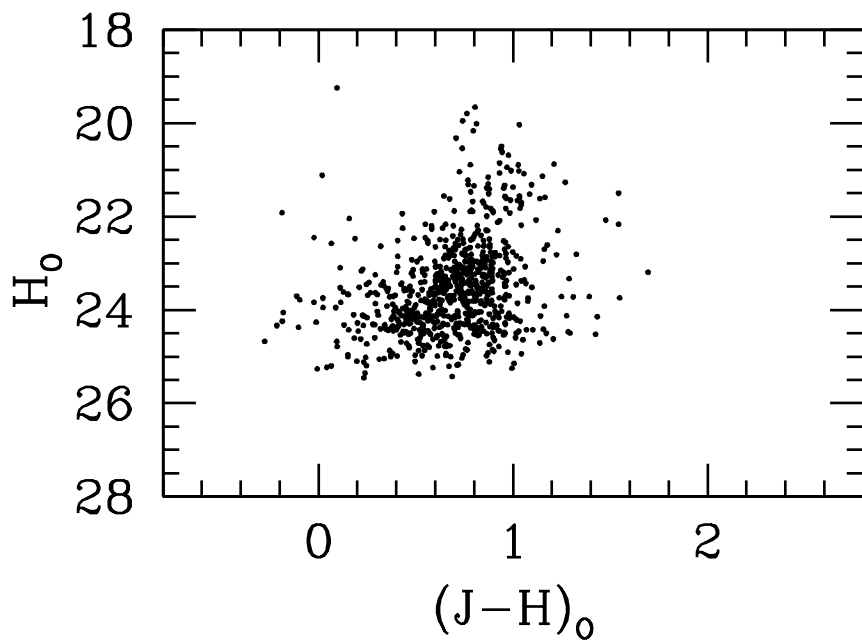
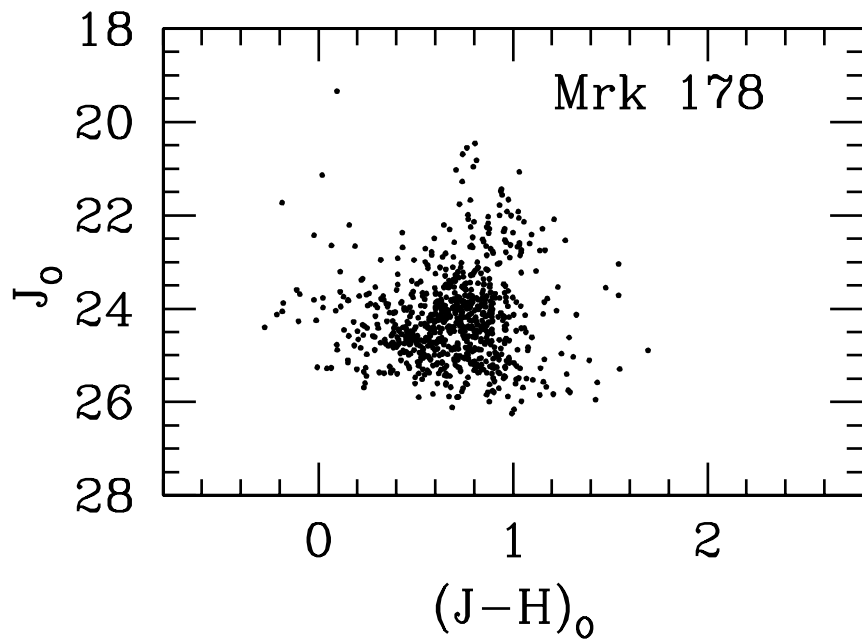


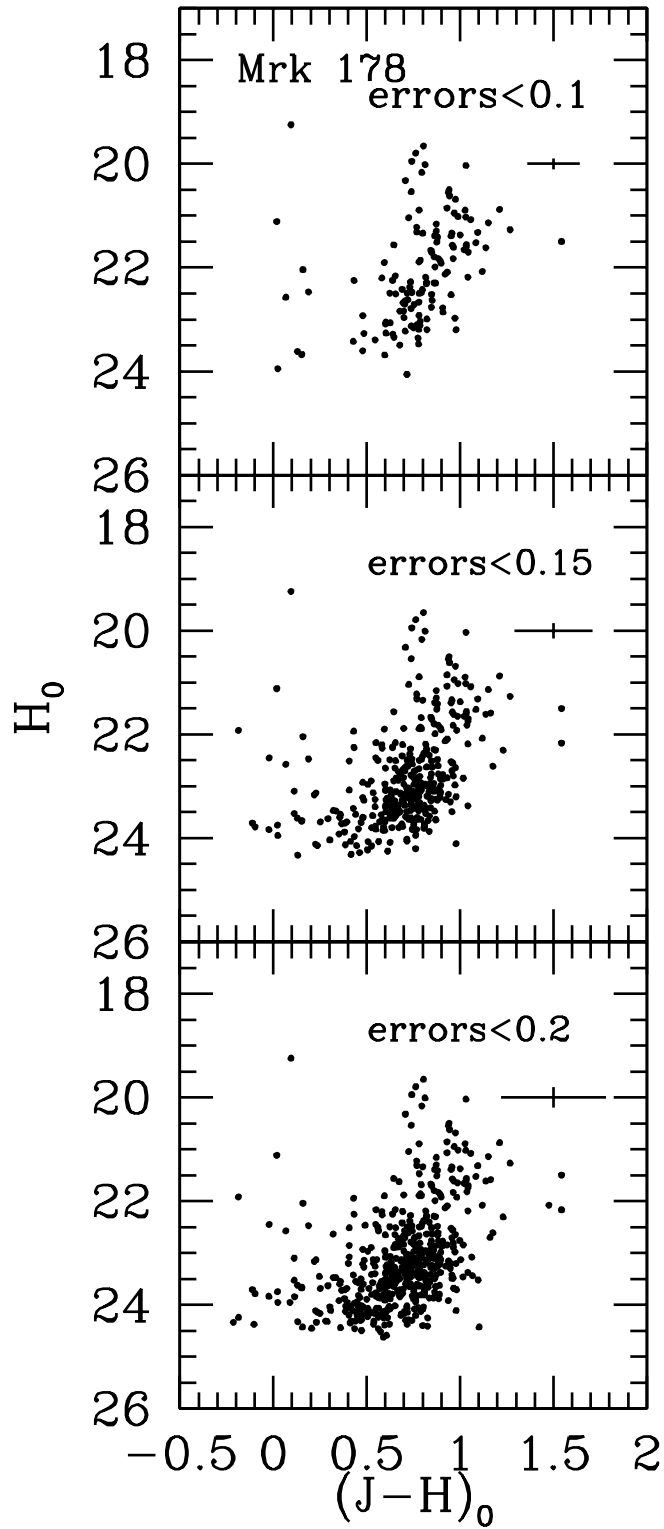


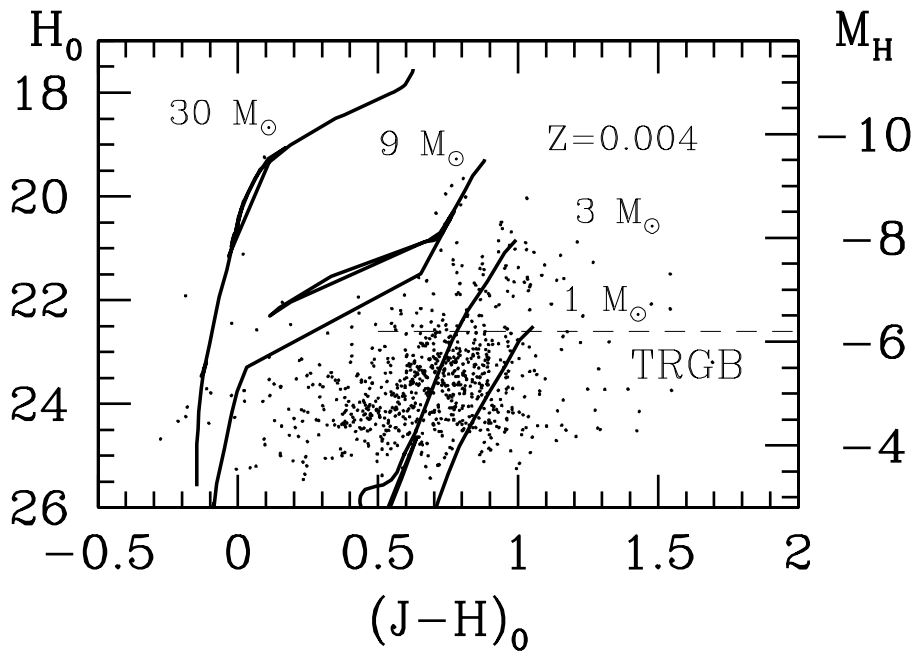
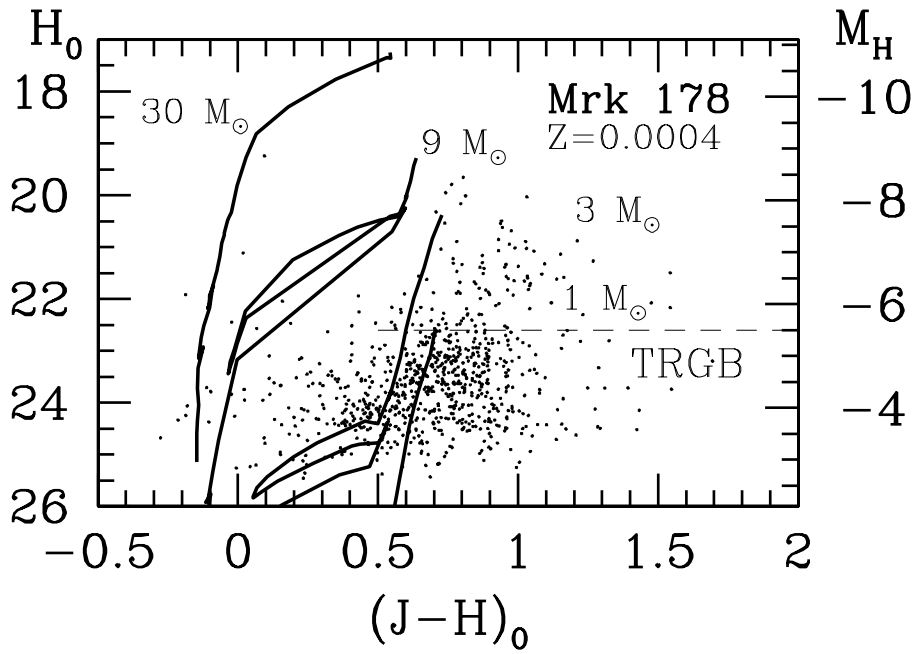


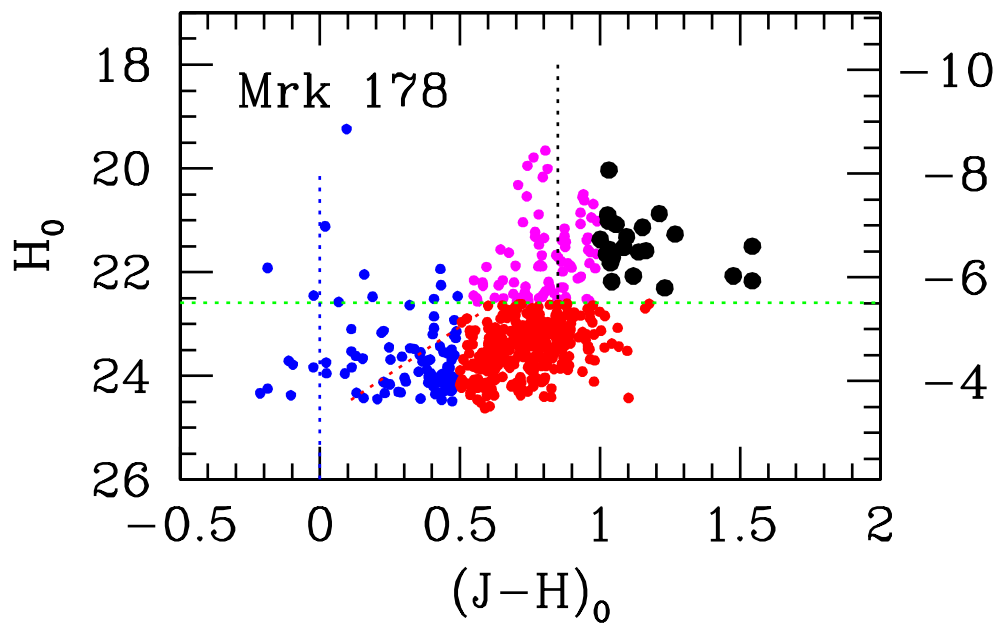
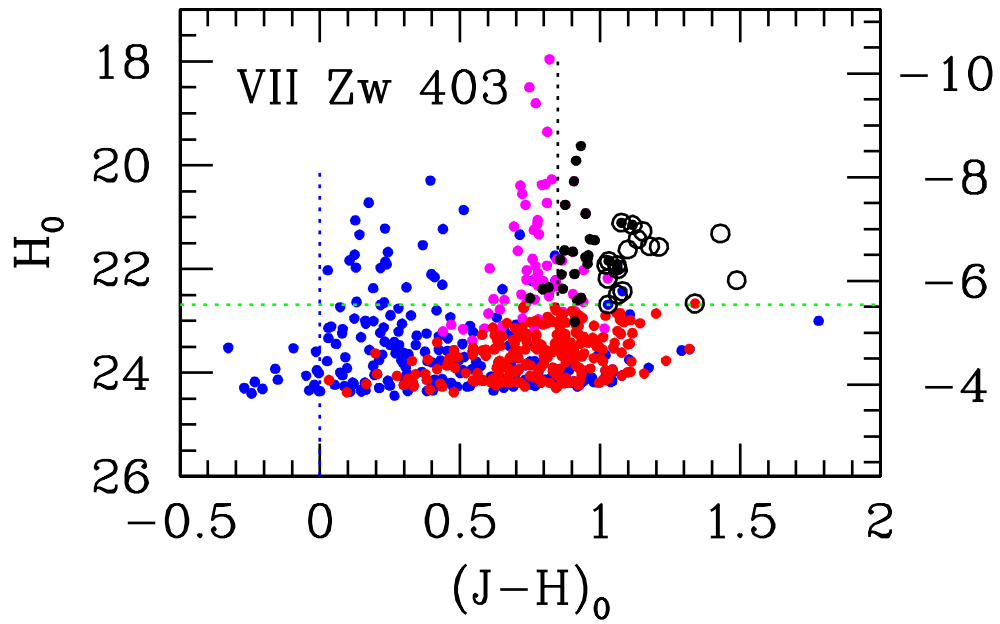


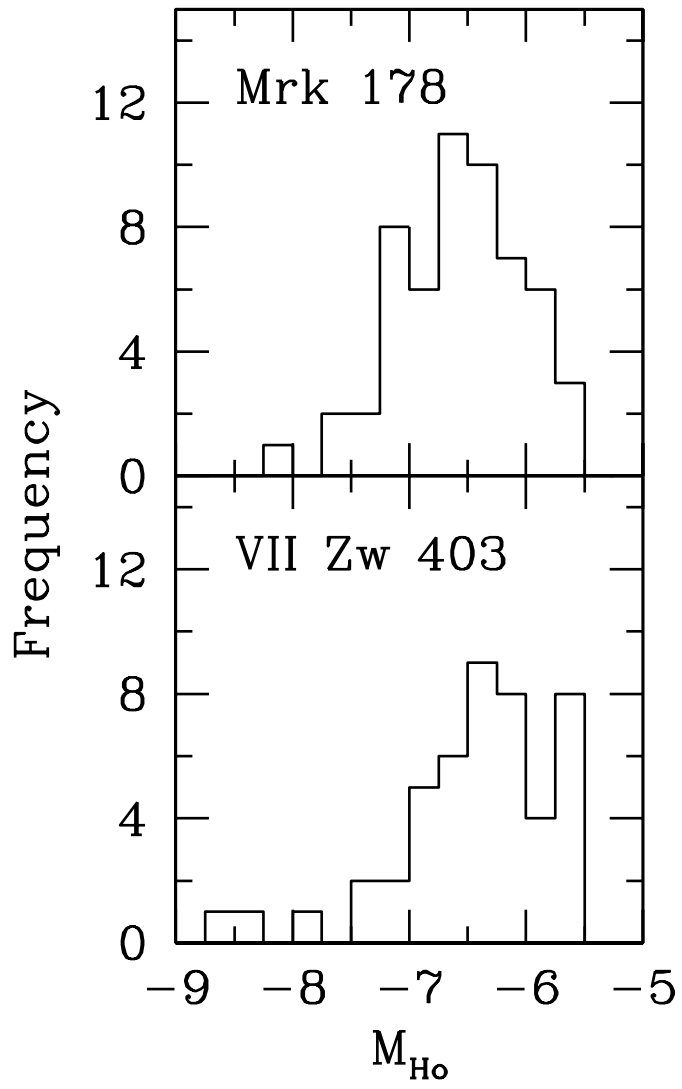








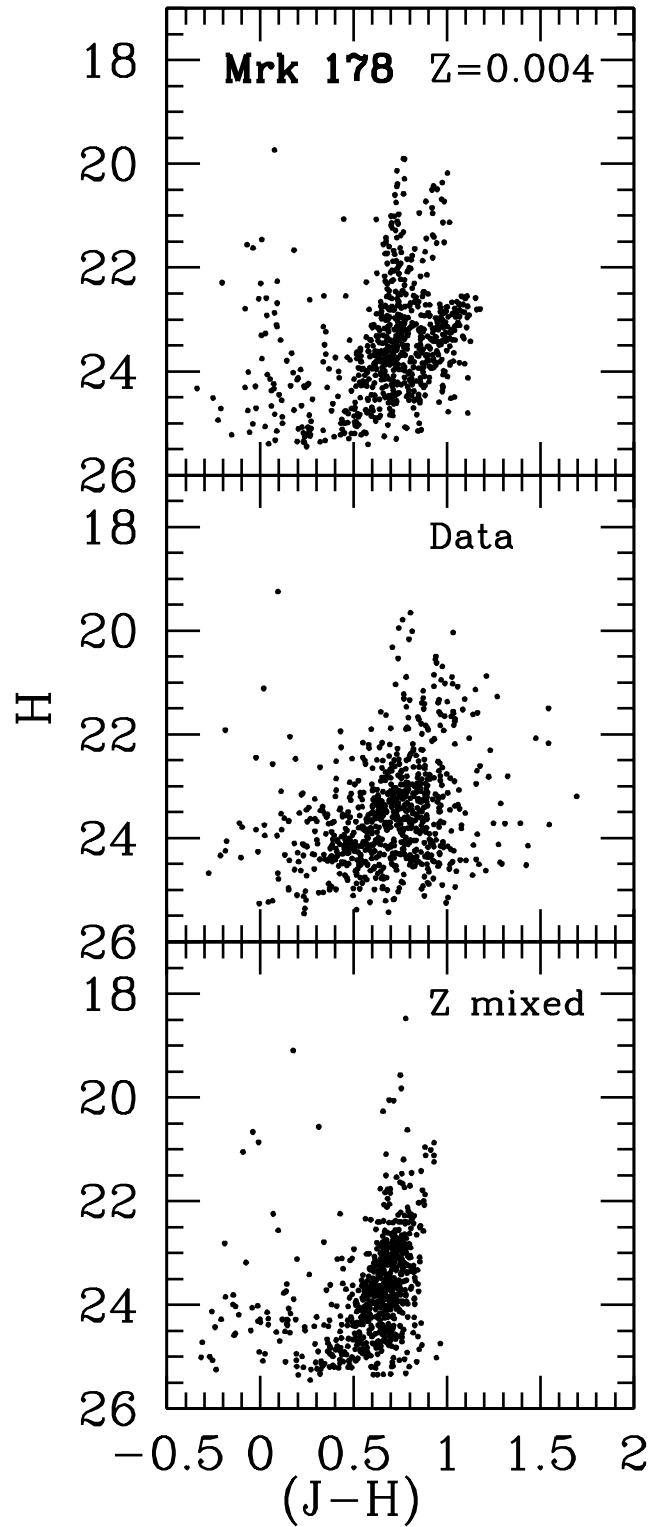






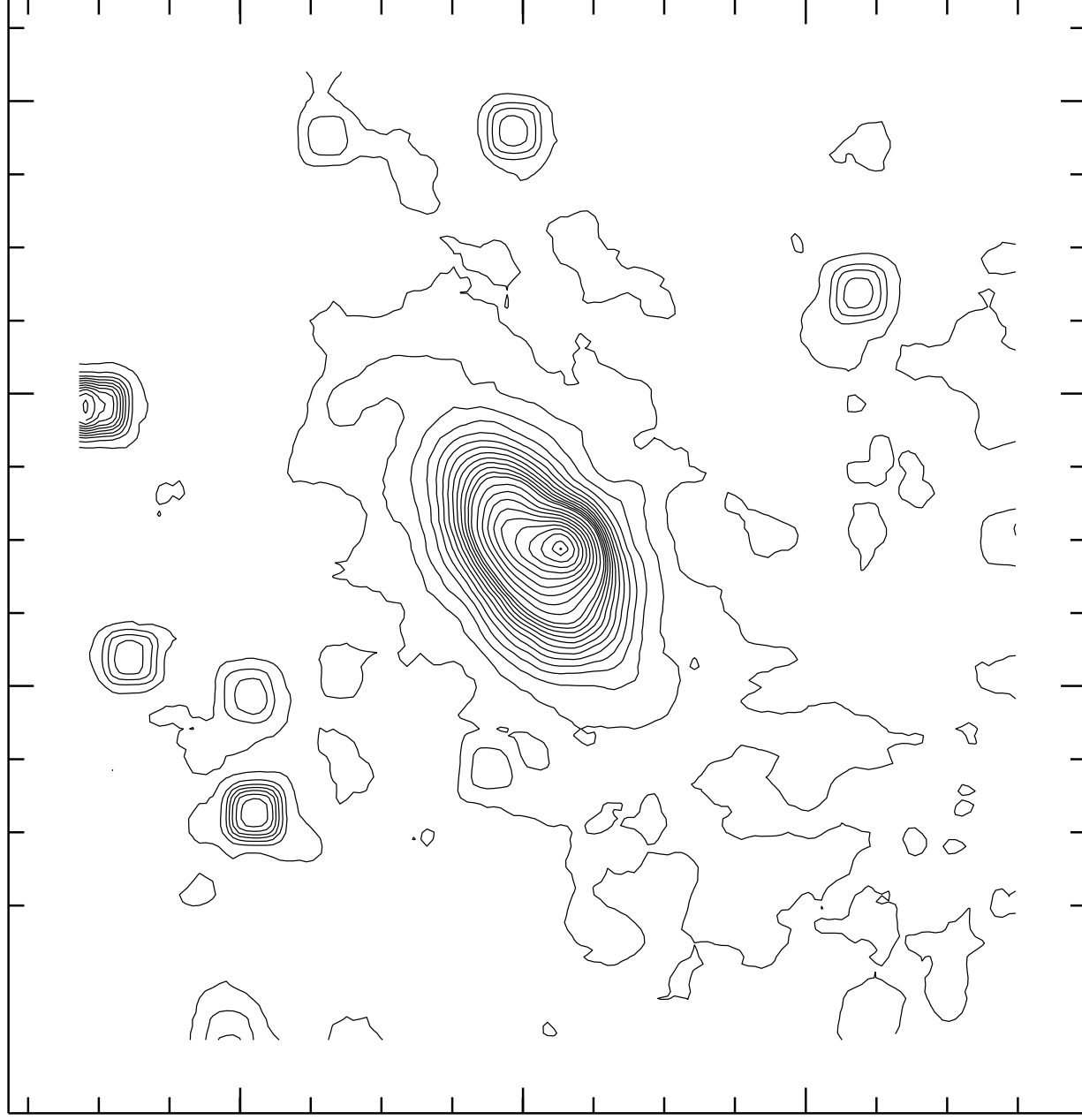
This figure "sl\_mrk\_fig12.gif" is available in "gif" format from:

<http://arxiv.org/ps/astro-ph/0007417v1>



Frame: Mrk178dss

Ident: dss19234



49.26

49.24

49.22

173.38 173.36

173.34

Position (RA---TAN )